ARL-TR-9180 • Apr 2021

DEVCOM ARMY RESEARCH LABORATORY

Sputtered Platinum (Pt) Electrode Development for Lead Zirconate Titanate (PZT) Piezoelectric Microelectromechanical Systems (MEMS) Devices

by Daniel M Potrepka, Robert R Benoit, Glen R Fox, Matthew L Chin, Ryan Q Rudy, and Jeffrey S Pulskamp

NOTICES

Disclaimers

The findings in this report are not to be construed as an official Department of the Army position unless so designated by other authorized documents.

Citation of manufacturer's or trade names does not constitute an official endorsement or approval of the use thereof.

Destroy this report when it is no longer needed. Do not return it to the originator.

ARL-TR-9180 ● APR 2021

Sputtered Platinum (Pt) Electrode Development for Lead Zirconate Titanate (PZT) Piezoelectric Microelectromechanical Systems (MEMS) Devices

Daniel M Potrepka, Robert R Benoit, Matthew L Chin, Ryan Q Rudy, and Jeffrey S Pulskamp
Sensors and Electron Devices Directorate, DEVCOM Army Research Laboratory

Glen R Fox
Fox Materials Consulting, LLC

REPORT DOCUMENTATION PAGE

Form Approved
OMB No. 0704-0188

1. REPORT DATE *(DD-MM-YYYY)*	2. REPORT TYPE	3. DATES COVERED (From - To)
04-14-2021	Technical Report	1 January 2019–30 September 2020

4. TITLE AND SUBTITLE
Sputtered Platinum (Pt) Electrode Development for Lead Zirconate Titanate (PZT) Piezoelectric Microelectromechanical Systems (MEMS) Devices

5a. CONTRACT NUMBERS
W911NF1520118
W911NF2020160

5b. GRANT NUMBER

5c. PROGRAM ELEMENT NUMBER

6. AUTHOR(S)
Daniel M Potrepka, Robert R Benoit, Glen R Fox, Matthew L Chin, Ryan Q Rudy, and Jeffrey S Pulskamp

5d. PROJECT NUMBER

5e. TASK NUMBER

5f. WORK UNIT NUMBER

7. PERFORMING ORGANIZATION NAME(S) AND ADDRESS(ES)
DEVCOM Army Research Laboratory
ATTN: FCDD-RLS-EM
Adelphi, MD 20783-1138

8. PERFORMING ORGANIZATION REPORT NUMBER
ARL-TR-9180

9. SPONSORING/MONITORING AGENCY NAME(S) AND ADDRESS(ES)

10. SPONSOR/MONITOR'S ACRONYM(S)

11. SPONSOR/MONITOR'S REPORT NUMBER(S)

12. DISTRIBUTION/AVAILABILITY STATEMENT
Approved for public release; distribution unlimited.

13. SUPPLEMENTARY NOTES
ORCID IDs: Daniel M Potrepka, 0000-0002-0528-1038; Robert R Benoit, 0000-0002-3728-6706

14. ABSTRACT

The AJA ATC 2200 sputtering tool in the US Army Combat Capabilities Development Command Army Research Laboratory's cleanroom provides an option for platinum (Pt) 111 electrode deposition. Bottom electrodes deposited at 500–800 °C and 800–1000 Å thickness were characterized by four-point probe, X-ray diffraction (XRD), and atomic force microscopy. The Pt 111 had a minimum 222 rocking curve full width at half maximum (FWHM) of 1.6° ± 0.1° at 600 °C. To evaluate the impact of the Pt bottom electrode on devices, 5800 ± 75 Å PZT and 1000 Å IrO_2 top electrodes were deposited. The IrO_2/PZT/Pt film stacks were characterized by XRD, spectroscopic ellipsometry, capacitance, polarization, and breakdown voltage measurements. The PZT{100} rocking curve FWHM range was $6.3° < \Omega < 11.5°$, the 6.3° minimum for PZT on 500 °C AJA Pt. The electrical properties (nominally similar to those for PZT on 500 °C Pt from the Evatec Clusterline tool used previously) are dielectric constant 1300 ± 100 and percent loss tangent 2.5 ± 0.15 at 0 kV/cm DC bias field (310 ± 50 and 0.62 ± 0.5, respectively, at 350 kV/cm DC bias field), remnant polarization (Pr) 22 ± 2 μC/cm^2, and breakdown voltage (field) 35 ± 5 V (612 ± 88 kV/cm).

15. SUBJECT TERMS
lead zirconate titanate, piezoelectric capacitor, electrical and physical properties, platinum bottom electrode, characterization

16. SECURITY CLASSIFICATION OF:			17. LIMITATION OF ABSTRACT	18. NUMBER OF PAGES	19a. NAME OF RESPONSIBLE PERSON
a. REPORT	b. ABSTRACT	c. THIS PAGE			Daniel M Potrepka
Unclassified	Unclassified	Unclassified	UU	75	19b. TELEPHONE NUMBER (Include area code) (301) 394-0389

Contents

List of Figures

List of Tables

Acknowledgments

Daniel M Potrepka gratefully acknowledges James L Mulcahy for the many process discussions, the AJA ATC 2200 sputtering system and Clusterline setup, and overall maintenance support, Jaron Kropp for technical support and throw distance measurements, Robert A Burke for general cleanroom support, and Steven Isaacson for device fabrication. Funding for this work was provided by US Army contract numbers W911NF1520118 and W911NF2020160.

1. Introduction

Over the last three decades, the degree of miniaturization made possible by microelectromechanical systems (MEMS) technology has significantly improved the functionalities of motion-sensing applications. This leveraging of MEMS technology has expanded to applications spanning the detection of gases, magnetic fields, electromagnetic radiation, and many more.[1] In this timeframe, MEMS switches have provided a small form factor to replace electromechanical relays capable of reliably routing 0 Hz/DC to hundreds of gigahertz signals.[2] Within the field of microfluidics, lead zirconate titanate (PZT) can be used for making pumps and valves. For acoustic applications, piezoelectric micromachined ultrasonic transducers can be used for both sending and receiving ultrasound. Within optics, bending mode actuators can be used for making spectrometers (Fabry–Perot and Fourier transform infrared [FTIR]) and mirrors as well as coherence modifying devices.[3] Consumer applications further drive the piezoelectric MEMS industry, fulfilling many of the requirements of future smart devices including low power requirements, small volume, high performance, ease of manufacture for the Internet of Things (IoT), 5G, and camera lenses.[3,4]

In parallel, MEMS resonators have emerged to touch fields such as electronic timing and filtering, energy harvesting, and a wide range of resonant sensors, creating many industrial successes that often build upon novel academic research. Among these advances are devices for such applications as accelerometers, gyroscopes, inertial measurement units, biosensors, bolometers, gas sensors, magnetometers, micromechanical filters, microresonator-based timing systems, microresonators, microphones, pressure sensors, resonant energy harvesting, resonant sensors, and ultrasonic transducers.[1] Resonators with multifrequency generation at the device level are highly desired for multiband, reconfigurable, and compact wireless communications.[5] High-performance switchable resonators with high quality factor (Q) could dramatically reduce the power consumption, simplify processing circuits, and occupy less footprint for applications in future advanced RF front-end systems.[6]

Acceleration measurements are of great significance due to their extensive applications in military/industrial fields. In recent years, scientists have been pursuing methods to improve the performance of accelerometers.[7] Accelerometers capable of measuring acceleration, tilt, and vibration or shock are used in a diverse range of applications from wearable fitness devices to industrial platform stabilization systems. The latest MEMS capacitive accelerometers are finding use in applications traditionally dominated by piezoelectric accelerometers and other sensors. Applications such as condition-based monitoring, structural health

monitoring, asset health monitoring, vital sign monitoring, and IoT wireless sensor networks are areas where next-generation MEMS sensors offer solutions. The bandwidth and g-range can span up to those typical of accelerometers used in applications such as tactical weapons (<1 kHz bandwidth, 6g) and craft navigation (>300 Hz bandwidth, 15 g).[8]

Materials requirements for piezoMEMS applications are analyzed to determine size, weight, power, and cost for device quality and electrical performance with, among other factors, maintenance and improvement of the piezoMEMS microwave to millimeter wave dielectric constant and tuning, with high Q and strong piezoelectric coefficients.[9]

Prior investigations of the US Army Combat Capabilities Development Command Army Research Laboratory into PZT deposition have shown the importance of the filmstack processes on the electrical properties of PZT films deposited for device applications.[10] Procedures used to create the surface for the film stack, such as whether depositing directly on the Pt of the bottom electrode versus using nucleation and Ti-seed layers between the Pt and the PZT, or even the preparation of the Pt surface itself prior to the chosen PZT film process, can produce markedly different results. Careful studies of a variety of such combinations of film stacks and Pt surface conditions have been studied in a previous report.[11] These studies included physical characterization of the PZT film stacks and electrical analysis of devices produced from PZT and associated seed and nucleation layers on a virgin Pt electrode surface in vacuum versus on a reannealed Pt surface that was exposed to air prior to deposition.

This report describes the implementation of the AJA ATC 2200 sputtering system (hereafter referred to as AJA) to produce Pt bottom electrodes for sputtered PZT piezoMEMS devices. Up to this point, the Pt has been fabricated using the Process Module #4 (PM4) in the Evatec Clusterline (CLN) as described in Fox et al.[12] The tests performed in Fox et al.[12] along with process control monitoring of Ti and Pt resistance and 111 Pt texture established a highly optimized Pt 111 sputtered film process in the CLN. The current characterizations and tests seek to determine if a satisfactory electrode material is obtained with the AJA process. The materials characterization and electrical tests on PZT metal-insulator-metal (MIM) test capacitors used here are similar to those described in Strnad et al.[13] and Potrepka et al.[14]

The alternative AJA Pt process is desired to serve as a backup for depositing Pt sputtered electrodes. Having this additional capability for Pt films protects against potential process downtime resulting from age effects and wear and tear on the CLN. The AJA also offers an expanded substrate temperature range beyond that of

the CLN, up to 800 °C, which may provide a competitive advantage for improved Pt 111 texture that could in turn increase electrical performance. This work will explore a 500–800 °C temperature variation for AJA Pt deposition to qualify the AJA Pt process for the rigorous requirements of DEVCOM Army Research Laboratory piezoMEMS devices for Army systems such as phase shifters, filters, resonators, and in particular, gyroscopes.[10,15–18] The AJA Pt thickness was calibrated by comparing step height measurements for different deposition times and comparing the associated sheet resistances with a standard. Pt structure was analyzed by X-ray diffraction (XRD), and surface roughness by atomic force microscopy. PZT was deposited on the bottom electrodes. Its structure was characterized by XRD and thickness measured by ellipsometry. Electrical characterization was performed on MIM capacitor devices formed by depositing a top IrO_2 electrode. Results were compared with CLN-deposited devices to meet qualification and acceptance standards for devices used in ARL programs.

2. Experiment

2.1 Ti Process Control Monitor (PCM) and TiO_2 for the AJA Pt Deposition

The starting substrates for all the process wafers consisted of commercially supplied 150-mm-diameter, single crystal, (100) Si wafers on which 500 nm of thermal SiO_2 was grown. A four-Si-wafer × 15-min conditioning of the Ti target was performed at 1 kW, 40 °C, and 30 sccm Ar (2.8E-3 mbar). Then a hexagonal {0001}-textured Ti PCM test sample was sputter deposited onto SiO_2 in the CLN Ti sputtering module (260-mm-diameter Ti target at 99.99% purity, 50-mm target-substrate distance) by using a DC cathode power of 0.5 kW, Ar flow rate of 30 sccm (2.8E-3 mbar), and substrate temperature of 40 °C. This resulted in a Ti thickness of 20 nm after a deposition time of 35 s. The sheet resistance of the PCM was verified to be less than 60 Ω/sq. Then Ti was deposited, using the same deposition conditions as the PCM, on wafers from the same commercial thermal SiO_2 on Si batch. A furnace anneal at 750 °C for 30 min, using an O_2 flow rate of 3 SLM, converted the {0001}-textured Ti to 32 nm thick, rutile structure, {100}-textured TiO_2 as described in a previous report.[14]

2.2 AJA Pt

AJA ATC 2200 Co-sputter Deposition System with 4-inch-diameter shuttered Pt target, 99.99% pure, was prepared for Pt bottom electrode sputtering for piezoMEMS devices on 150-mm Si 100 wafers. Starting conditions for the AJA

are compared to those for the CLN-sputtered Pt in Table 1. Due to the larger, off-axis target-substrate distance tilted to aim at the wafer center (throw distance 176.5 mm vs. concentric, axial 50-mm target-substrate distance for the CLN) and lower DC power (200 W vs. 500 W) compared to the CLN, the AJA deposition time is more than five times as long for the CLN (450 s vs. 67 s). The deposition pressures of the AJA and CLN are similar. The AJA wafer rotates in-plane about its central axis at 60 rpm while in process. The CLN does not provide a substrate rotation feature. An example of the AJA process flow for 1000-Å Pt thickness and a deposition temperature of 600 °C is shown in Table 2 and plotted in Fig. 1. The temperature ramp accounts for most of the approximate 3.5-h process time. In contrast, because the CLN Pt sputter chamber remains at the deposition temperature of 500 °C and wafers cycle into and out of it without the need for heating and cooling steps, that process flow lasts approximately 3 min as shown in Table 3.[14]

Table 1 AJA and CLN sputtered Pt process conditions (left to right): DC power, deposition time, deposition temperature, Ar pressure, Ar flow, nominal target substrate distance, and wafer in-plane rotation speed about the wafer's central axis

Deposition system	P_{DC} (W)	t_{DEP} (s)	T (°C)	P_{Ar} (mTorr)	Ar flow (sccm)	Z (mm)	Rotation speed (rpm)
AJA	200	450	500–800	5	30	176.5	60
CLN	500	67	500	3	50	50	0

Table 2 Running time of AJA sputtered-platinum (nominal 1070 Å, 600 °C) process steps

h:min	Process step
0:00	Process program begins, T → 500 °C
0:01	500 °C, 15 min Soak, T → 550 °C
0:17	550 °C, 15 min Soak
0:32	Ramp to 600 °C begins, 600 °C, 15 min soak begins
1:28	Ar Plasma on, shutter opens 10 s later
1:36	Ar Plasma off, ramp to 550 °C begins
1:37	550 °C, 15 min soak, ramp to 500 °C begins
1:52	500 °C, 15 min soak, ramp to 450 °C begins
2:07	450 °C, 15 min soak, ramp to 400 °C begins
3:02	400 °C, 15 min soak, temperature free fall begins
3:32	Process program ends

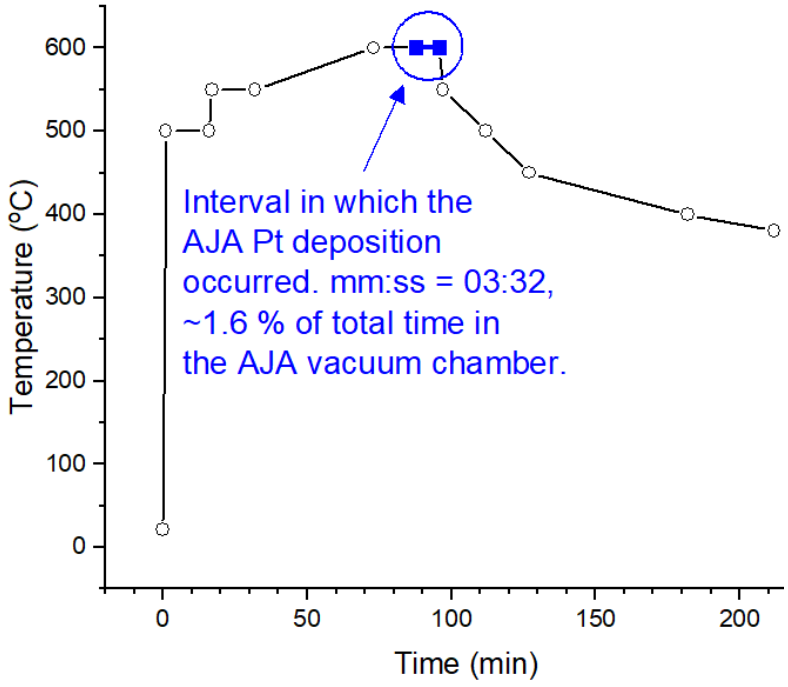

Fig. 1 Temperature vs. time plot for the AJA deposition at 600 °C, 107 nm

Table 3 CLN times for sputtered-platinum (1000 Å, 500 °C) process steps

Sequence	Time (s)	Pt_0500W_50sccm_0067s
Step 1	30 (nominal)	Pump out
Step 2	60 (nominal)	Ar 30sccm, 60s, (40°C)
Step 3	67	Pt_0500W_Ar50_67s_500C
Step 4	30 (nominal)	Pump out

The AJA Pt thickness was calibrated by step profilometer measurement obtained at room temperature for a Kapton tape–defined step on a Si wafer. The process for depositing this Pt film used the conditions and flow in the aforementioned tables but with the substrate at room temperature (21 °C).

The sheet resistances of PCM1 and PCM2, 1.97 and 1.45 Ω/sq, respectively (Table 4), obtained in the Four Dimensions Model 280SI Sheet Resistivity Measurement System, were consistent with the 1.41 Ω/sq value for standard Pt (Wafer 1 in Table 4) deposited in the CLN by a PCM-controlled process with the conditions in Table 3. The five-digit number appended to the Sample IDs is the laser scribe on the wafer. From here on, samples will be referred to by the first digit only (viz. Sample 1, Wafers 1–8, etc.) for convenience. The initial AJA deposition batch consisted of Wafers 2–5 with substrate temperatures in the range 500–800 °C

and 352-s deposition time (Table 4). Their estimated Pt thickness of 812 Å is assigned based on the same deposition time as PCM1, neglecting impact of their varied elevated-temperature depositions on TiO_2 compared to 21 °C on native oxide (NatOx) for PCM1. A second batch, Wafers 6–8, was deposited at fixed temperature and time of 600 °C and 450 s, respectively. A Pt thickness of 1000 Å was computed to have an approximate deposition time of 423 s based on a scaling comparison of sheet resistances for PCM1 and PCM2 (Fig. 2). However, due to device considerations, 450 s was chosen to ensure that at least 1000 Å was deposited after accounting for error bars in the thickness calibrations. At the beginning of each batch, a conditioning wafer was deposited at the starting temperature for the first wafer. Then, Pt was deposited onto the wafers prepared with TiO_2 as described previously.

Table 4 Bottom Pt electrode characteristics (left to right): wafer number (and laser scribe after hyphen), deposition surface beneath the Pt, Pt deposition temperature, time (t_{DEP}), film thickness (s), sheet resistance (R_s), and rocking curve full width at half maximum (RC-FWHM). The Pt thickness was measured at five points (center and 2.54 cm from top, left, bottom, and right of wafer, flat at bottom) for PCM1 and PCM2 and derived for Wafers 2–8.

Wafer ID	Substrate	T (°C)	t_{DEP} (s)	S (Å)	R_s (Ω/sq)4,~8,82pts	Pt 111 RC-FWHM (°)
PCM 1	NatOx/Si	21	352	812 ± 58	1.97 ± 0.02	N/A
PCM 2	NatOx/Si	21	450	1070 ± 74	1.45 ± 0.01	N/A
1-12139[a]	TiO_2	500	67	1000 ± 50	1.41 ± 0.02	2.45 ± 0.06
2-12621	TiO_2	800	352	812 ± 20	1.95 ± 0.05	1.98 ± 0.05
3-12774	TiO_2	700	352	812 ± 20	1.98 ± 0.05	2.01 ± 0.02
4-12619	TiO_2	600	352	812 ± 20	1.88 ± 0.06	1.86 ± 0.02
5-12538	TiO_2	500	352	812 ± 20	1.88 ± 0.04	2.59 ± 0.04
6-12434	TiO_2	600	450	1070 ± 50	1.13 ± 0.03	1.59 ± 0.05
7-12438	TiO_2	600	450	1070 ± 50	1.13 ± 0.03	1.61 ± 0.05
8-12505	TiO_2	600	450	1070 ± 50	1.13 ± 0.03	1.45 ± 0.05

[a] Wafer 1 was deposited in the Clusterline (CLN). All others are AJA depositions.

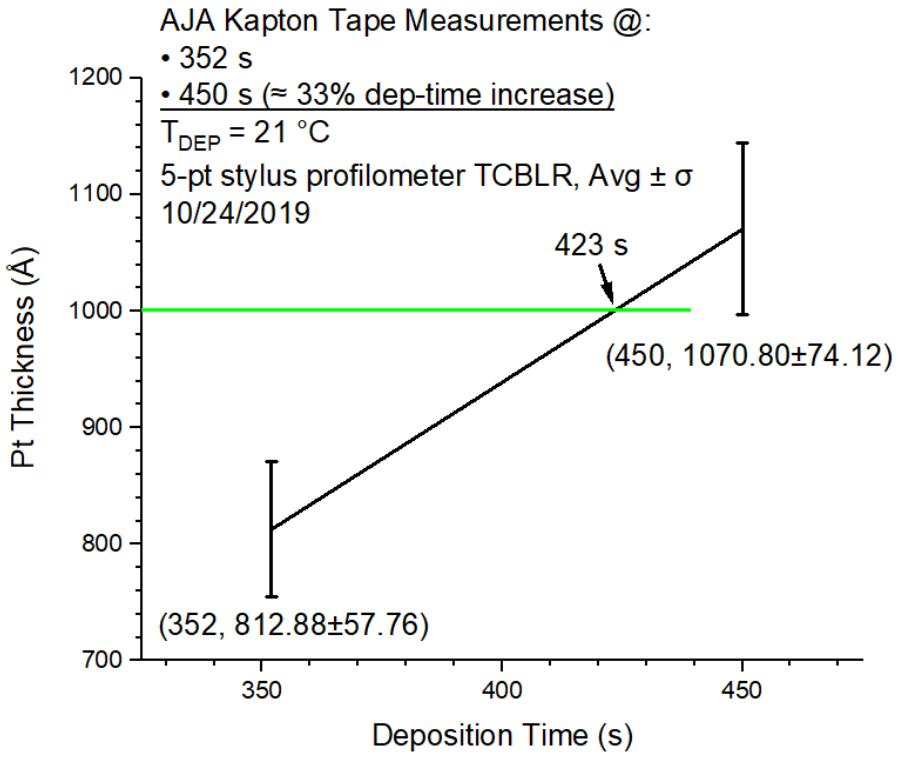

Fig. 2 AJA Pt thickness calibration

Sheet resistances were obtained in the Four Dimensions Model 280SI Sheet Resistivity Measurement System. The measurements were taken at 81 locations distributed uniformly across all but the outer approximate half inch of the 150-mm wafer's Pt film surface. XRD measurements of 10°–90° θ–2θ scans and Pt 222 rocking curves were obtained for Pt deposited at 500–800 °C for 352 s, and with (estimated) thickness of 812 ± 20 Å at five locations on the wafer: center and 1.5 inches out from center toward top, bottom, left, and right (wafer flat down) in a Malvern Panalytical X'pert3 CuKα X-ray diffractometer.

2.3 Atomic Force Microscope (AFM)

Surface roughness was measured using a Veeco Dimension V Nanoscope AFM on the deposited Pt surfaces. Each sample was exposed to a nitrogen gas stream to remove any large particulates and then visually inspected using an optical microscope to check for any potential remaining particles or residues. The AFM was used in tapping mode, with a scan area of 5 µm × 5 µm, a scan rate of 0.5 Hz, tip velocity of 2.5 µm/s, sampling rate of 512 samples per line, and height/Z limit of approximately 3–4 µm to ensure that the full range of roughness, topography changes, and incidental particles could be accommodated.

2.4 PZT Clusterline

In preparation for processing, the chamber temperatures of the Ir and PZT chambers were increased to 500 °C and 640 °C, respectively. Power and Ar conditioning protocols were performed on the PZT chamber. In parallel, the Ti chamber was reconditioned (4 Si wafers × 15 min) as described in the process wafers preparation description in Section 2.1. The sheet resistance of the PCM was 56.11 ± 0.86 Ω/sq, meeting specifications for the combination of Ti purity and thickness. Appendix A provides tables describing the preparation and procedures for Ti chamber (PM1) conditioning process flow and sequence (Tables A-1 and A-2), Ti PCM deposition flow and sequence (Tables A-3 and A-4), the measured chamber conditions for Ti conditioning (Table A-5), Ir chamber (PM3 used for Pt heating) initial temperature ramp flow and sequence (Tables A-6 and A-7), Ir chamber pressure conditions during the temperature ramp (Table A-8), and PZT chamber (PM6) temperature ramp and conditioning information (Tables A-9 through A-16).

Next the process for obtaining the PZT layer was initiated. The first PZT depositions were performed in PM6 on four PZT-coated preconditioning wafers deposited at 2 kW, 600 s, and 450 °C with no Ti seed or nucleation layers. After inspection to verify that no particulates formed on the surface, the deposition process was performed on the process wafers. The tables in Appendix A provide more detail about the deposition process, procedures, and conditions (Tables A-17 through A-29).

The process performed for the PZT depositions in the CLN included reheating (rebake) of the AJA Pt in the PM3 Ir chamber to prepare the surface for Ti seed deposition. This heating in PM3 was at 500 °C, 10 min at 0 sccm (no gas flows), (1 ± 0.5)E-4 mbar average chamber pressure.[*] The Pt surface was refreshed in this manner to drive off moisture and other physisorbed contamination on the Pt wafers after removal from the Pt sputtering system and exposure to air that can occur prior to loading into the CLN PM3.

Next, the Ti seed layer was sputter deposited in the PM1 Ti chamber of the CLN (260-mm-diameter Ti target at 99.99% purity, 50-mm target-substrate distance) at 250 W, 40 °C, 30 sccm Ar, 3 s, (2.80 ± 0.05)E-3 mbar process pressure (2E-7 ultimate vacuum pressure).

Then the PZT was deposited in the PM6 PZT chamber of the CLN (300-mm PZT target at 99.9% purity, $Pb_{1.22}Zr_{0.52}Ti_{0.48}O_3$) without a vacuum break during chamber transfer. After pumpdown, establishing initial gas flows, and firing of the plasma,

[*] This process is usually done in the Clusterline PM4 chamber, which is nominally identical to PM3, but PM4 was down at the time.

PZT nucleation and volume depositions were performed at 2 kW, matching capacitor settings Cs = 550 and Csh = 900, and 640 °C substrate temperature. The 640 °C substrate temperature was chosen to achieve sufficiently high breakdown strength as determined in earlier preliminary studies of the PZT deposition versus temperature.

A PZT nucleation layer deposition was performed next using 80 sccm Ar gas flow for 60 s. Then a PZT volume deposition was performed using alternating (56, 0) sccm and (54, 4) sccm (Ar, O_2) flows at 5 s each, looped for 80 cycles with nominal (2.67 ± 0.02)E-3 mbar process pressure above a 3E-8 mbar base (ultimate vacuum) pressure. The wafers were then removed from the process chamber and cooled for 60 s in the ambient vacuum of the wafer transfer module of the CLN, then returned to the (5E-3 mbar) low-vacuum conditions of the loading-chamber wafer cassette for eventual retrieval.

The PZT-depositions were performed in the order of Wafers 1–8. Times between depositions are given in Appendix A (Table A-11). After deposition the wafers were inspected visually to check the film color and uniformity and to verify that no buildup of particles from the shields was developing over time. Then a photograph was taken of each wafer surface (Appendix B, Figs. B-1a through B-1h). The artifact near the flat of Wafer 1-12139 (CLN 500 °C) is a masking done in the AJA and was not used for this study. PZT thickness was obtained by spectroscopic ellipsometry measurements using a J.A. Woollam Model M-2000 F Spectroscopic Ellipsometer with x-y stage and WVASE software, 32 measurement points, 30–60 Å surface roughness, Tauc Lorentz modeled PZT, no PZT-Pt intermix, and a modeled Pt-annealed surface under the PZT. [19,20] XRD 10°–90° θ-2θ scans and PZT {100} rocking curves were obtained in the Malvern Panalytical System prior to the IrO_2 top electrode depositions. XRD measurement locations were at five points on the wafer: center and 1.5 inches out from center toward top, bottom, left, and right (wafer flat down).

2.5 IrO_2 Top Electrode

The IrO_2 top electrode deposition was performed in the CLN PM3 Ir chamber (using an iridium sputtering target with 300-mm diameter and 99.9% purity) at 450 °C, 1000 W, Ar 100 sccm, O_2 60 sccm, 35 s for 1000 Å thickness. Prior to depositing the process wafers, preconditioning was performed under process condition to ensure sheet resistance approximately 9 Ω/sq, consistent with the IrO_2 thickness.[21] Table A-30 in Appendix A shows the process used. Values of the deposition parameters are tabulated in Appendix A (Table A-31). After deposition, the IrO_2 films were annealed in a quartz tube furnace at 650 °C for 30 min in 3 SLM

O_2.[21] XRD θ-2θ scans were performed for $10° \leq 2\theta \leq 90°$ in the Malvern Panalytical System at the wafer center.

The PZT was patterned and etched to define MIM capacitors. After the PZT ion milling and a short dilute wet etch to remove potential residual PZT not visible under the optical microscope, electrical measurements were performed. Then additional XRD measurements were made at an unmilled IrO_2/PZT/Pt region remaining for such testing purposes in the center of the process wafers.

2.6 Characterization

All of the electrical measurements were made at five locations, center and near the top, bottom, left, and right of the test wafers in the voltage range of –20 V < V < 20 V. The PZT thickness was used to compute the electric field (E = 350 kV/cm) that samples were subjected to during the electrical measurements. Capacitance and loss tangent as a function of voltage were obtained using an Agilent 4192A 5 Hz–13 MHz LF impedance analyzer with 0.5-V oscillator level. Polarization versus voltage measurements were performed on a Radiant Technologies Inc Precision Premier II materials analyzer. Four polarization versus voltage/E-field (PE) curves were generated. The waveform for polarization was a 20-Hz triangle wave. A bipolar positive PE curve was generated for 0 to 20 to –20 to 0 V. A unipolar positive PE curve was generated for 0 to 20 to 0 V. A bipolar negative PE curve was generated for 0 to –20 to 20 to 0 V. Finally, a unipolar negative PE curve was generated for 0 to –20 to 0 V. The breakdown voltage was measured using a Keithley 2400 source meter with 1-V steps at about 1-s intervals between steps.

3. Discussion and Analysis

3.1 Pt Characterization

According to the room temperature sputtering tests, the AJA Pt on NatOx/Si(100) growth rate was calibrated to be 2.31 and 2.38 Å/s for 352 and 450 s deposition times, respectively. This assumes linear scaling as shown in Fig. 2.

The 10°–90° XRD scans in Fig. 3 were measured at wafer center. They show the Pt 111 and 222 orientation peaks for the AJA Pt deposited at 500–800 °C, 352 s deposition time. The Fig. 3 data is a quick measurement tilted out of the diffraction plane by a tilt angle of approximately 0.5° in Chi that suppresses the Si 400 peak, but in the process diminishes the Pt peaks so that they are only useful for rough qualitative comparisons that quickly identify the Pt peak locations but are not intended for numerical intensity comparisons. Similar peaks were obtained at

measurement locations about 1.5 inches from the top, bottom, left, and right wafer edges (wafer flat down at 6 o'clock positions). The rocking curves obtained for optimized measurement conditions for the Pt 222 rocking curve are shown in Fig. 4. From Table 4, R_s is 1.88–1.98 Ω/sq for AJA Samples 2–5, 352-s deposition time (812 ± 20 Å Pt thickness estimated from room-temperature Pt thickness monitor). R_s is 1.13 ± 0.03 Ω/sq for AJA Samples 6–8, Pt depositions at 600 °C, 450-s deposition time (1070 Å estimated Pt thickness from room-temperature Pt thickness monitor). The R_s for CLN Pt (Wafer 1), 1.41 ± 0.02 Ω/sq, is consistent with these results. The rocking curve full width at half maximum RC-FWHM for 500 °C AJA Pt (2.59° ± 0.04°) in Table 4 and Fig. 4 is similar to that for the CLN (2.45° ± 0.06°), indicating they have similar texture. There is a spread of RC-FWHM and peak intensity with temperature, indicating a change in texture of the microscopic structure that can be used to tailor the material properties in future development.

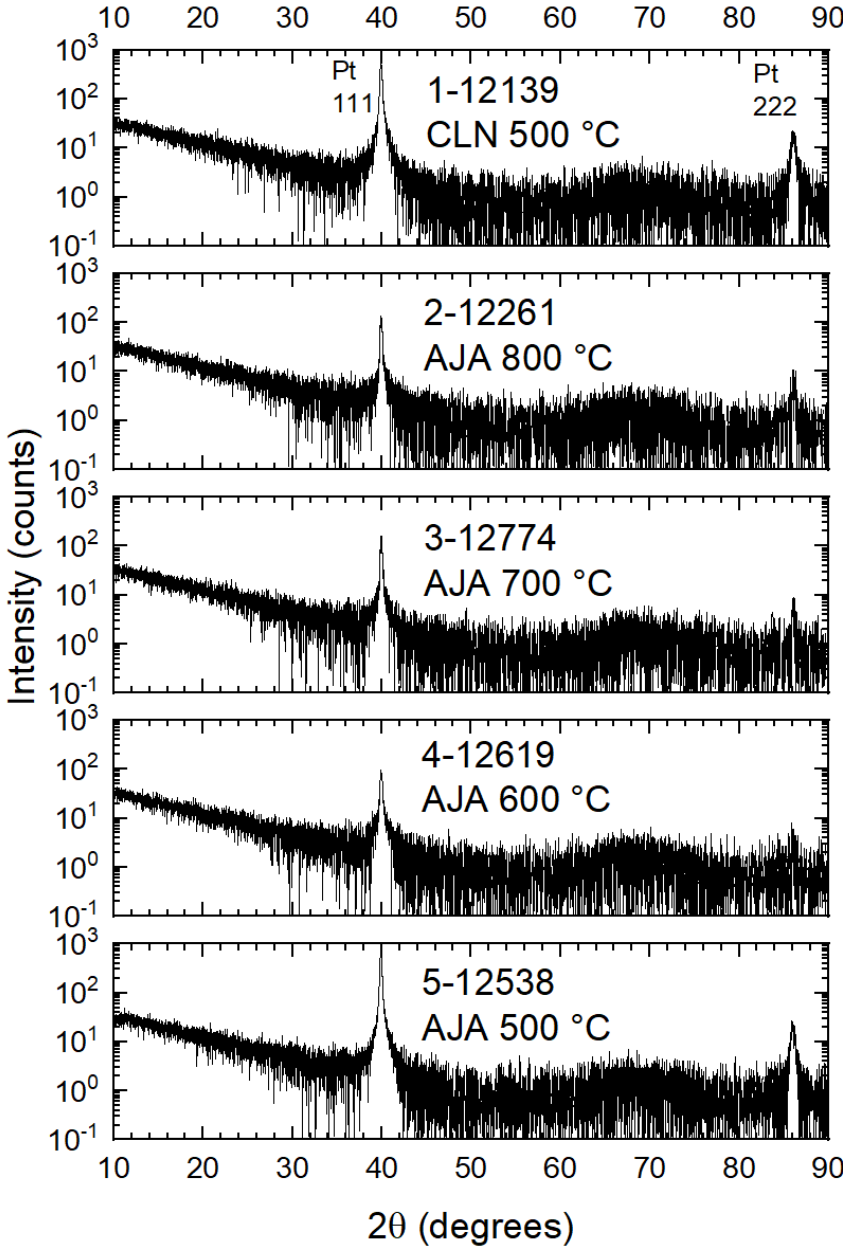

Fig. 3 XRD measured with 0.5° Chi tilt for AJA Pt 500–800 °C temperature variation and CLN 500 °C control sample

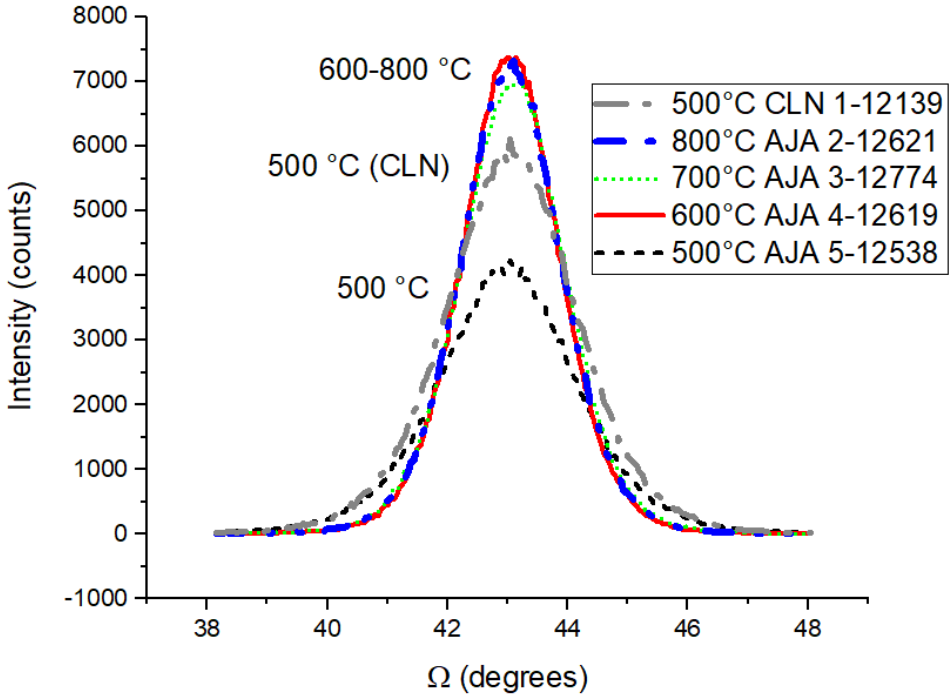

Fig. 4 Platinum 222 XRD RC-FWHM measured at the wafer center for the CLN 500 °C and AJA 500–800 °C samples

3.2 AFM

Table 5 surveys the roughness of the AJA Pt 111 500–800 °C versus that from the CLN 500 °C. Images of the AFM region sampled are shown in Appendix B (Figs. B-2a through B-2e). The surface roughness improvement is about a factor of 2 for maximum surface roughness (R_{max} ~20–30 nm to ~10 nm) and average roughness (R_a ~ 2 nm to 1 nm), and about a factor of 3 for root mean square (RMS) roughness (R_q ~ 3 nm to 1 nm) for AJA-sputtered Pt when increasing the temperature from 500 to 600 °C. However, there is little to no improvement from further temperature increase to 700 or 800 °C. Compared to the control process, it appears that the AJA sputter process is roughly on par with 500 °C CLN, which has R_q = 1.95 nm, R_a = 1.57 nm, and R_{max} = 16.5 nm values that are intermediate to those for AJA Pt at 500 and 600 °C. A substrate temperature difference between the CLN and the AJA could explain the difference between the 500 °C AJA and CLN microstructures.

Table 5 AFM surface roughness comparison for AJA Pt vs. standard CLN Pt (minimum values in bold)

Wafer sample	RMS roughness (R_q)	Average roughness (R_a)	Max roughness (R_{max})
Standard Pt wafer center	1.95 nm	1.57 nm	16.5 nm
Standard Pt wafer 1.3 cm from wafer edge	2.00 nm	1.61 nm	17.8 nm
AJA Pt wafer @ 500 °C center	2.91 nm	2.13 nm	29.4 nm
AJA Pt wafer @ 600 °C center	0.997 nm	0.782 nm	**9.10 nm**
AJA Pt wafer @ 700 °C center	**0.958 nm**	**0.740 nm**	12.2 nm
AJA Pt wafer @ 800 °C center	1.16 nm	0.890 nm	11.7 nm

3.3 PZT/Pt material characterization

The images of the surfaces of the deposited PZT films (Appendix B, Figs. B-1a through B-1h) are roughly similar in color and uniformity. Except for a minor asymmetry in coloring at about 2–3 cm from the center toward the flat for 4-12619 AJA 600 °C, there are no major differences. This spot had no noticeable effect on the measured local thickness. The Woollam spectroscopic ellipsometry in Table 6 shows that the PZT thickness for all the temperatures and the CLN control wafer is approximately 5800 Å.

Table 6 Thickness for PZT (T_{DEP} = 640 °C) obtained from Spectroscopic Ellipsometry (32 measurement points after outlier data point removal) and RC-FWHM

Sample ID	Deposition System	T_{Pt} (°C)	PZT Thickness (Å)	PZT 100 RC-FWHM (°)
1-12139	CLN	500	5784 ± 67	6.50 ± 0.05
2-12621	AJA	800	5816 ± 65	9.22 ± 0.05
3-12774	AJA	700	5802 ± 143	9.42 ± 0.05
4-12619	AJA	600	5810 ± 63	11.50 ± 0.05
5-12538	AJA	500	5782 ± 65	6.31 ± 0.05
6-12434	AJA	600	5771 ± 65	11.50 ± 0.05
7-12438	AJA	600	5783 ± 60	11.50 ± 0.05
8-12505	AJA	600	5771 ± 65	11.44 ± 0.05

XRD 10°–90° scans and RC-FWHM for PZT before top electrode deposition are shown in Figs. 5 and 6, respectively. For comparison, 10°–90° plots similar to Fig. 5 were obtained after IrO_2 top electrode and anneal (Fig. 7). These were indexed for composition in Figs. 7a and b. The plot of the PZT {001} peak for all the samples after top electrode deposition is displayed in Fig. 7c.

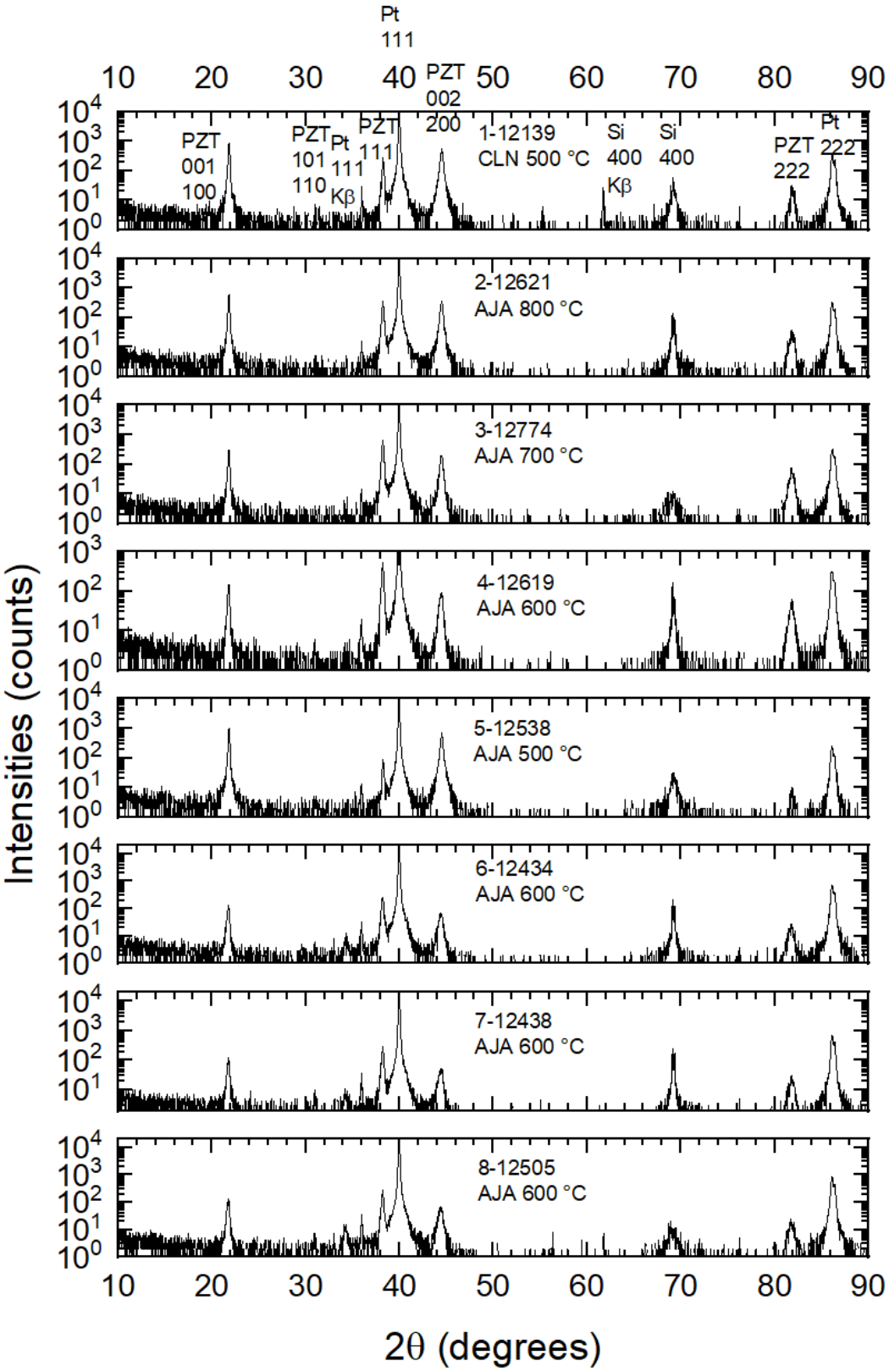

Fig. 5 PZT on Pt XRD (no top electrode) measured with 0.5° Chi tilt

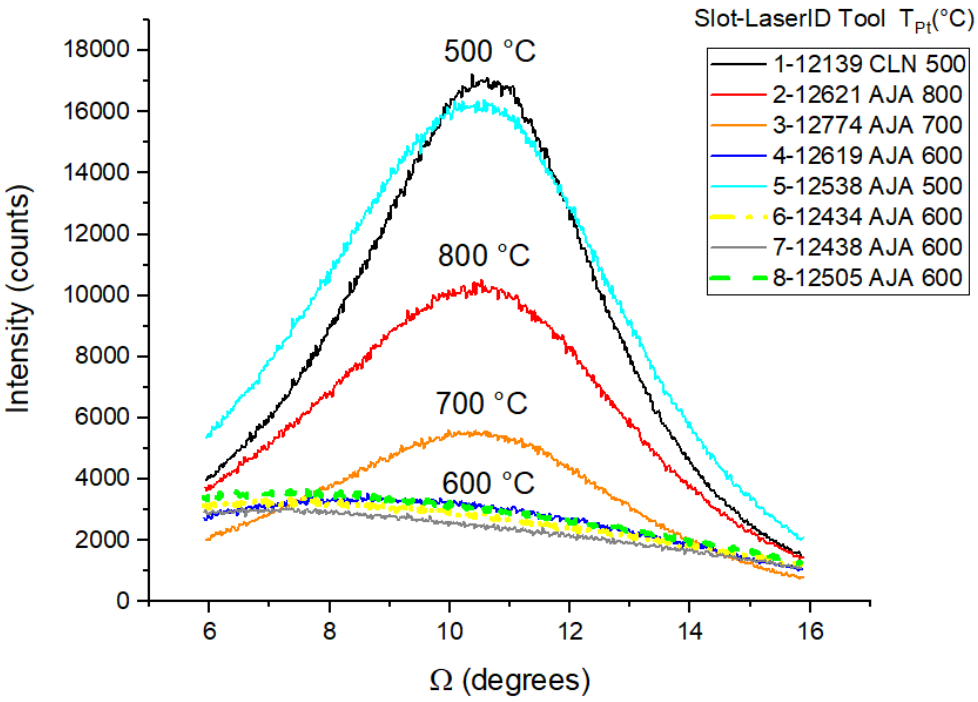

Fig. 6 PZT {001} XRD RC-FWHM for PZT deposited at 640 °C on Pt that was deposited at temperatures shown and measured at the wafer center for CLN and AJA samples with Pt deposition temperatures shown (no top electrode)

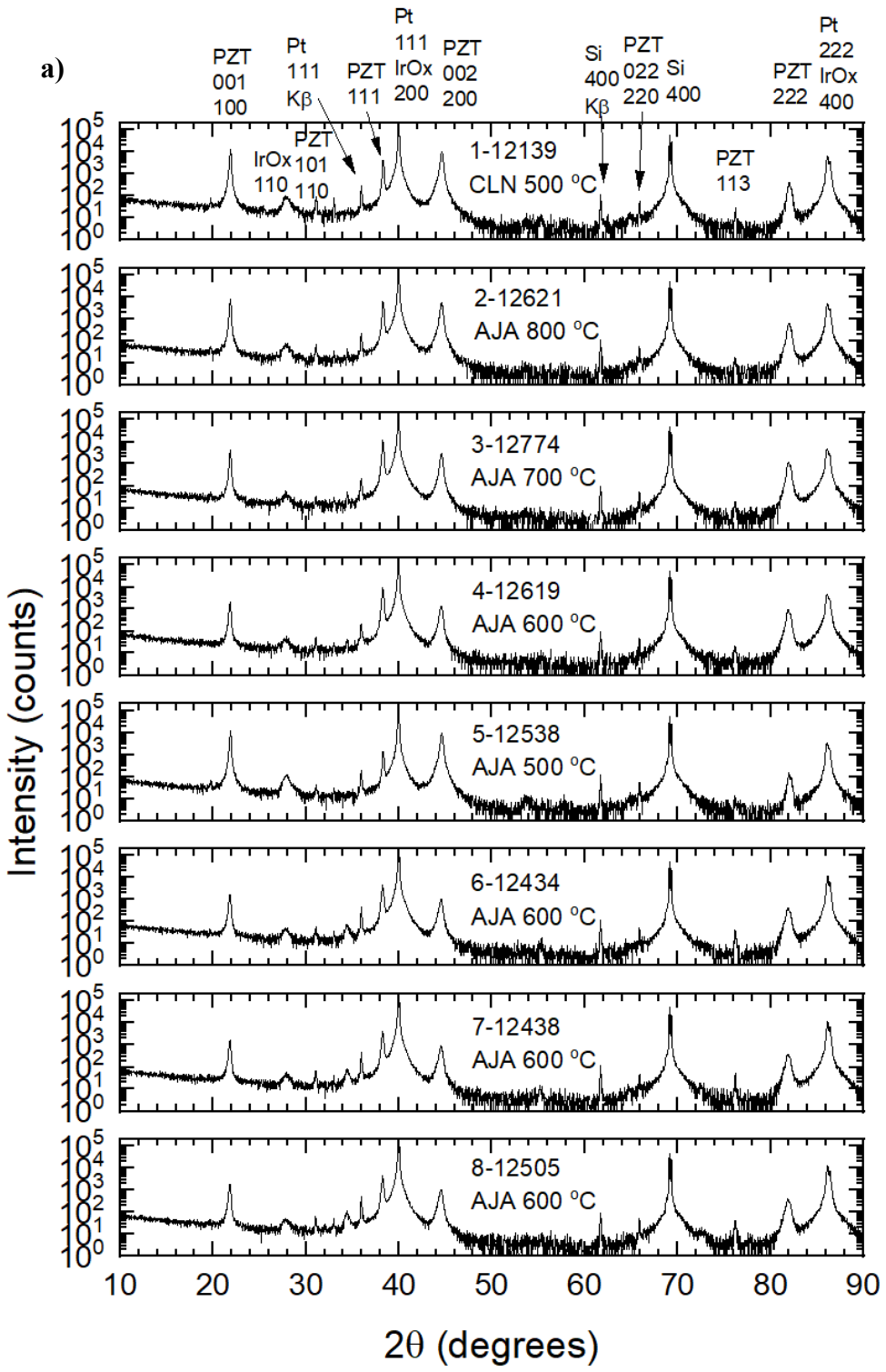

Fig. 7 XRD through the IrO_2/PZT/Pt unpatterned top-electrode regions after MIM patterning of 1000 Å (Sample 1), ~812 Å (Samples 2–5) and ~1070 Å (Samples 6–8) Pt thicknesses for a) $10° \leq 2\theta \leq 90°$, b) $27° \leq 2\theta \leq 36°$ intermediate range peaks, and c) the $21.5° \leq 2\theta \leq 22.5°$ PZT {001} peak range. The Pt-deposition substrate temperature is shown for each curve.

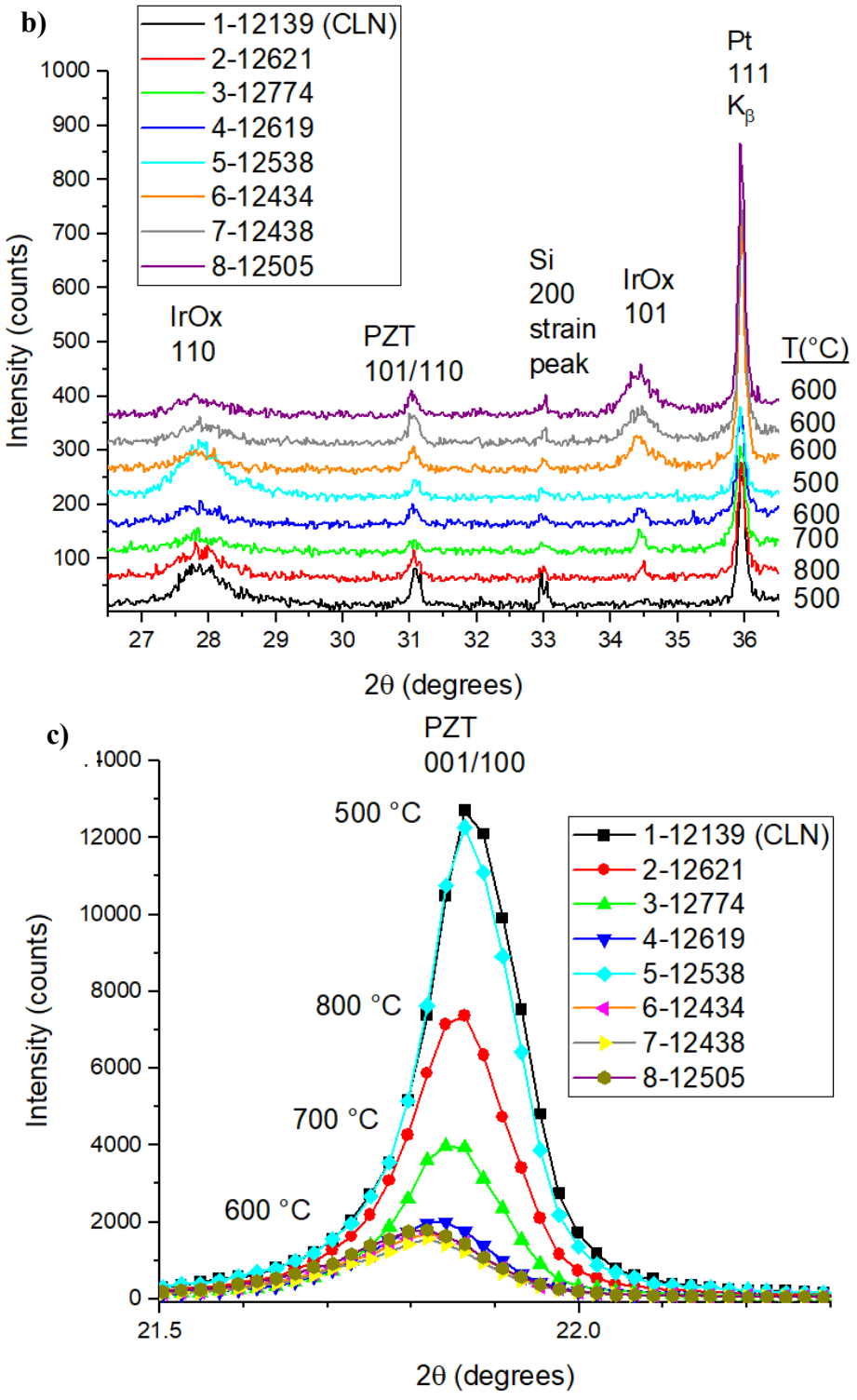

Fig. 7 XRD through the IrO_2/PZT/Pt unpatterned top-electrode regions after MIM patterning of 1000 Å (Sample 1), ~812 Å (Samples 2-5) and ~1070 Å (Samples 6-8) Pt thicknesses for a) 10° ≤ 2θ ≤ 90°, b) 27° ≤ 2θ ≤ 36° intermediate range peaks, and c) the 21.5° ≤ 2θ ≤ 22.5° PZT {001} peak range. The Pt-deposition substrate temperature is shown for each curve (continued).

Table 6 shows the PZT 100 RC-FWHM for 500–800 °C versus CLN 500 °C before IrO_2 top electrode deposition. It is notable that the RC-FWHMs are to within instrumental resolution (Error Bars < 0.05°) comparable for AJA and CLN depositions at 500 °C substrate temperature (6.31° and 6.50°, respectively). The order of minimum to maximum PZT {001} RC-FWHM occurs for AJA Pt substrate temperatures 500, 700, 800, and 600 °C (Table 6 and Fig. 6), which may imply changes in PZT orientation with respect to the Pt temperature. Figure 8 is a correlation plot that shows the wafer order, Pt deposition temperature, Pt intensity, and Pt RC-FWHM. In general, the trend in PZT RC-FWHM appears uncorrelated to change in AJA Pt substrate temperature. The surface roughness does not necessarily correlate with grain size (which gradually increases with temperature as shown in Appendix B (Figs. B-2a through B-2e) or surface roughness (see Table 5). However, the larger surface roughness for the 500 °C depositions (AJA and CLN) may be contributing to their larger RC-FWHM and lower X-ray peak intensity for the Pt 100 peak analysis. Still, there does not appear to be a general trend for surface roughness dependence on PZT orientation.

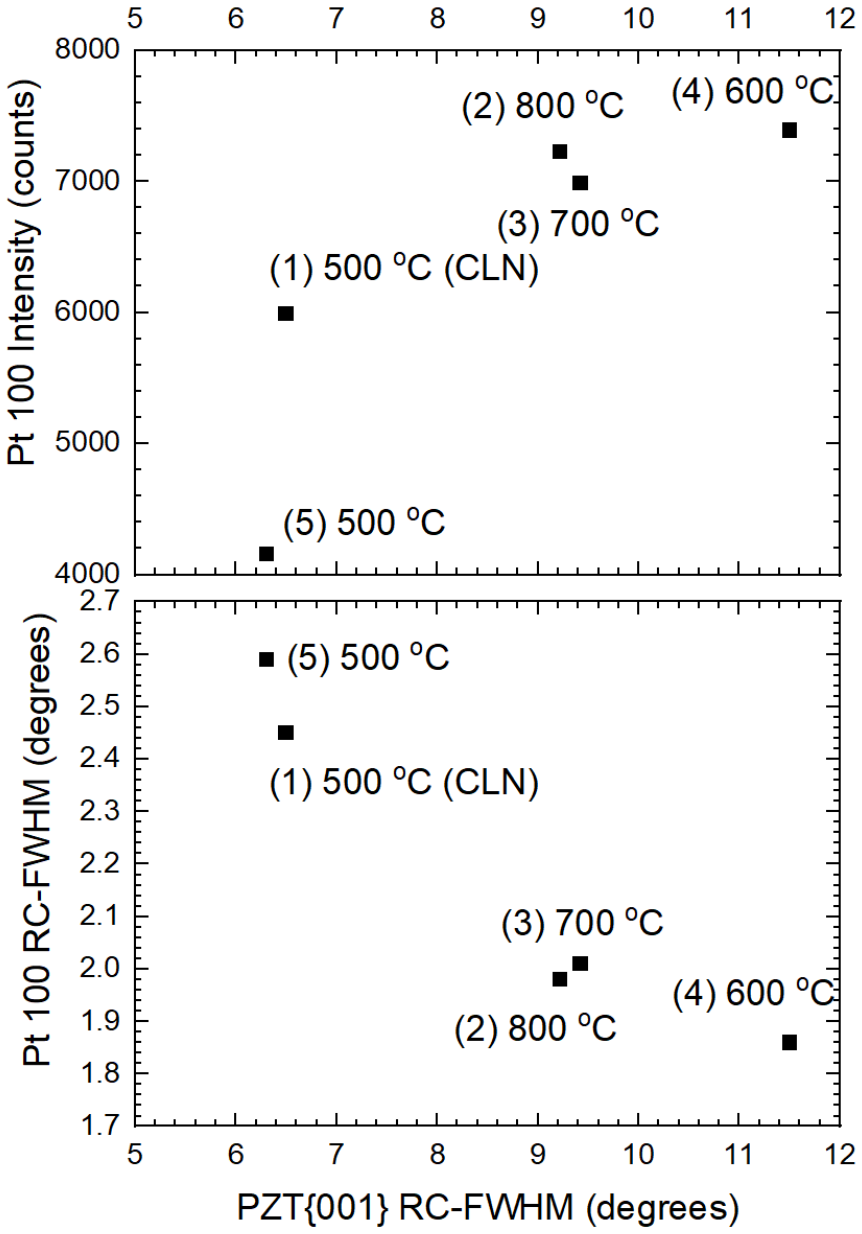

Fig. 8 Correlation of Pt 222 XRD intensity and RC-FWHM with PZT {001} RC-FWHM

3.4 PZT Electrical Characterization after MIM Capacitor Fabrication

The following conclusions are drawn based on the data shown in Tables 7 and 8. Overall breakdown strength is high (550 kV/cm through a maximum of 800 kV/cm for one of the AJA 600 °C samples). PZT electrical properties for the AJA Pt samples are good and generally exceed those for the CLN Pt sample. The wafers were not annealed after the top electrode etch, so imprint and etch damage could affect the electrical measurement. A sample with a 500 °C Pt top electrode,

Sample 9 shown at the bottom of Table 7 for comparison, has a lower P_{MAX} and Pr and much smaller hysteresis curve width $E_{c+} + E_{c-}$, indicating that the substitution of IrO_2 for Pt improves the piezoelectric behavior and pinning properties. However, the dielectric constant for the samples with IrO_2 top electrodes is generally somewhat lower than for Sample 9. For sample 5-12538, the minimum Ec for the AJA 500 °C and CLN 500 °C samples indicate the best interfaces, but the Pr is slightly reduced. The complete loops for these two cases for both bipolar and unipolar measurements at the wafer center are shown in Figs. 9a and 9e. Similar results were obtained at all five wafer locations. For Sample 6 (with AJA Pt 600 °C), the high $E_{c+} + E_{c-}$ and E_{BD} suggest that there is an interface layer.

Table 7 Electrical breakdown voltage, coercive fields, imprint, and remnant polarizations after top electrode etch (no anneal). Data for samples with 500 °C AJA Pt in bold. The breakdown voltages corresponding to E_{BD} are provided in Appendix C.

Sample ID	E_{BD} (kV/cm)	E_{c+} (kV/cm)	E_{c-} (kV/cm)	$E_{c+} + E_{c-}$ (kV/cm)	P_{MAX} (μC/cm²)	P_{r+} (μC/cm²)	P_{r-} (μC/cm²)
1-12139	**567 ± 121**	**29 ± 2**	**–29 ± 6**	**0.1 ± 6.9**	**42.0 ± 1.8**	**18.8 ± 1.7**	**–18.1 ± 3.3**
2-12621	554 ± 15	35 ± 2	–29 ± 3	6.0 ± 3.4	46.5 ± 1.9	21.9 ± 1.2	–23.1 ± 1.2
3-12774	624 ± 88	36 ± 4	–28 ± 3	7.2 ± 6.5	46.1 ± 2.8	20.9 ± 2.1	–22.2 ± 2.0
4-12619	544 ± 40	35 ± 3	–32 ± 5	3.3 ± 6.4	47.2 ± 3.0	23.3 ± 1.5	–25.1 ± 2.2
5-12538	**553 ± 59**	**30 ± 1**	**–29 ± 3**	**1.4 ± 2.8**	**42.0 ± 0.7**	**18.4 ± 1.0**	**–19.0 ± 1.4**
6-12434	797 ± 285	43 ± 12	–32 ± 1	10.6 ± 12.6	46.8 ± 3.1	22.3 ± 1.6	–24.9 ± 3.6
7-12438	619 ± 38	49 ± 25	–38 ± 12	11.4 ± 15.6	48.1 ± 33	21.9 ± 1.0	–23.9 ± 4.7
8-12505	596 ± 20	49 ± 19	–38 ± 11	10.2 ± 10.9	47.3 ± 5.6	21.0 ± 3.1	–24.9 ± 5.4
9-12147	580 ± 82	7±11	–10±12	–2.7±23.5	38.6 ± 1.4	3.5±1.4	–2.6±1.0

Note: 1-12139 = CLN Pt Bot E

1 bad Pr data point omitted for 7-12438, 2 for 8-12505.

9-12147 CLN Pt bottom electrode and AJA Pt (500 °C) top electrode. This data is added to the table for comparison.

Table 8 Dielectric constant and percent loss tangent at E = 0 and E = E_{MAX}

Sample ID	ε (0 kV/cm)	ε (350 kV/cm)	% tan δ (0 kV/cm)	% tan δ (350 kV/cm)
1-12139	1398 ± 110	347 ± 19	2.8 ± 0.7	0.9 ± 0.9
2-12621	1316 ± 128	311 ± 31	2.3 ± 0.7	0.5 ± 0.8
3-12774	1284 ± 89	313 ± 45	2.3 ± 0.6	0.7 ± 0.8
4-12619	1286 ± 193	304 ± 47	2.5 ± 0.6	0.7 ± 0.9
5-12538	1307 ± 228	332 ± 18	2.6 ± 0.4	0.7 ± 0.4
6-12434	1266 ± 88	304 ± 59	2.5 ± 0.8	0.5 ± 0.6
7-12438	1232 ± 121	282 ± 64	2.5 ± 0.5	0.5 ± 0.6
8-12505	1220 ± 286	293 ± 94	2.4 ± 0.5	0.7 ± 0.7
9-12147	1431 ± 164	350 ± 80	2.5 ± 0.8	0.5 ± 0.5

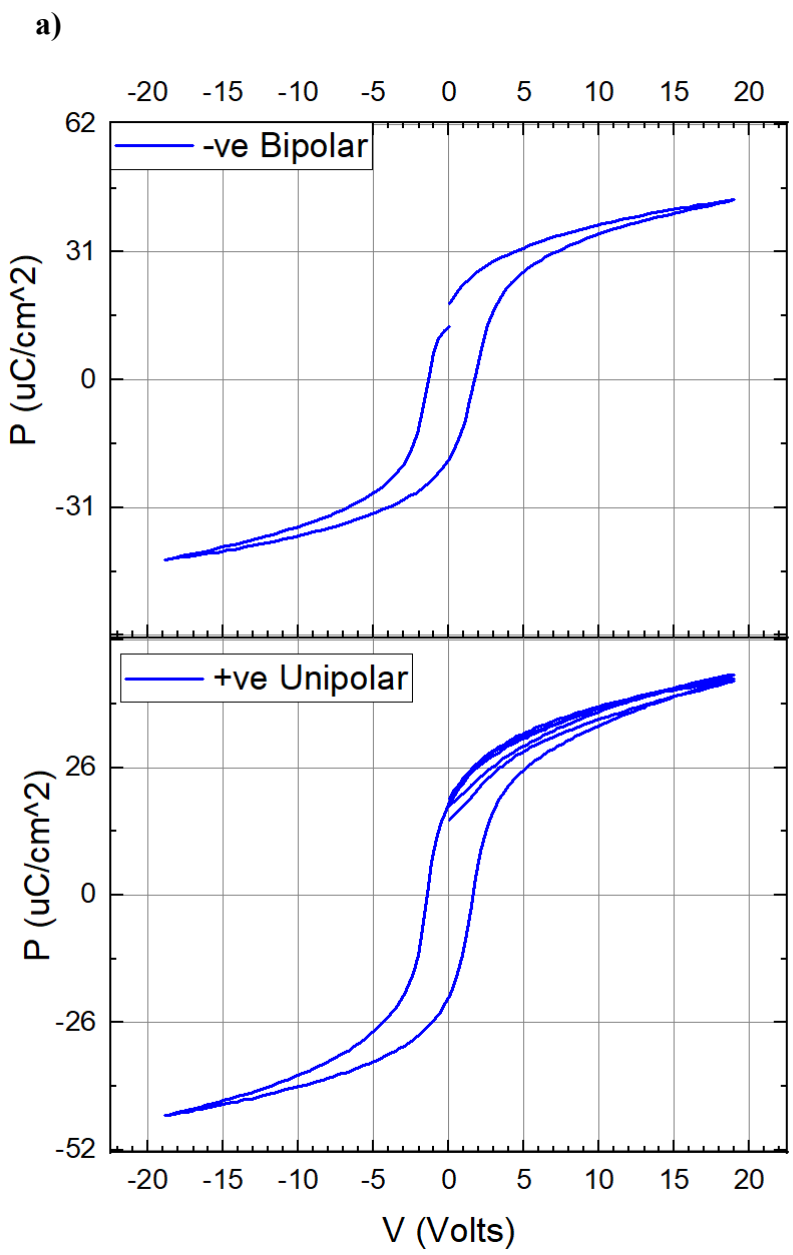

Fig. 9 a) Bipolar and unipolar polarization curves for Sample 1 PZT on CLN Pt (500 °C). b) Sample 2 PZT on AJA Pt (800 °C). c) Sample 3 PZT on AJA Pt (700 °C). d) Sample 4 PZT on AJA Pt (600 °C). e) Sample 5 PZT on AJA Pt (500 °C). f) Sample 6 PZT on AJA Pt (600 °C). g) Sample 7 PZT on AJA Pt (600 °C). h) Sample 8 PZT on AJA Pt (600 °C).

b)

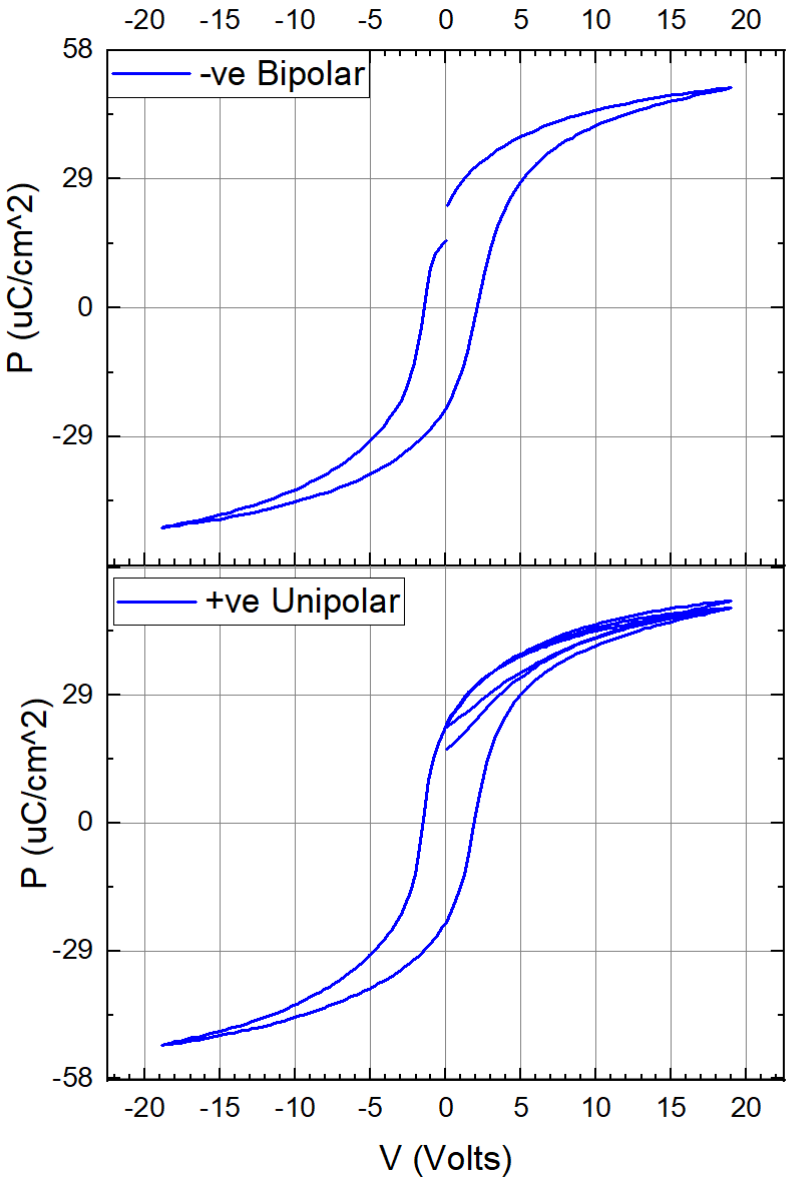

Fig. 9 a) Bipolar and unipolar polarization curves for Sample 1 PZT on CLN Pt (500 °C). b) Sample 2 PZT on AJA Pt (800 °C). c) Sample 3 PZT on AJA Pt (700 °C). d) Sample 4 PZT on AJA Pt (600 °C). e) Sample 5 PZT on AJA Pt (500 °C). f) Sample 6 PZT on AJA Pt (600 °C). g) Sample 7 PZT on AJA Pt (600 °C). h) Sample 8 PZT on AJA Pt (600 °C) (continued).

c)

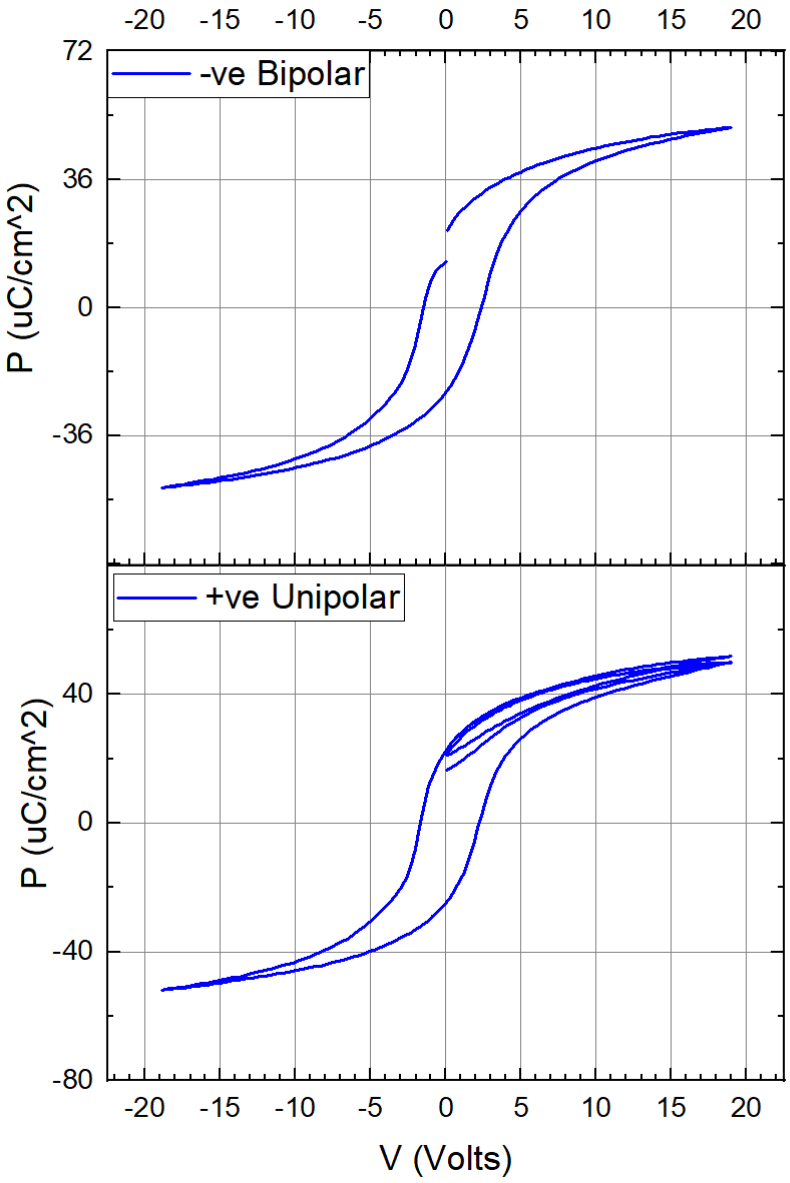

Fig. 9 a) Bipolar and unipolar polarization curves for Sample 1 PZT on CLN Pt (500 °C). b) Sample 2 PZT on AJA Pt (800 °C). c) Sample 3 PZT on AJA Pt (700 °C). d) Sample 4 PZT on AJA Pt (600 °C). e) Sample 5 PZT on AJA Pt (500 °C). f) Sample 6 PZT on AJA Pt (600 °C). g) Sample 7 PZT on AJA Pt (600 °C). h) Sample 8 PZT on AJA Pt (600 °C) (continued).

d)

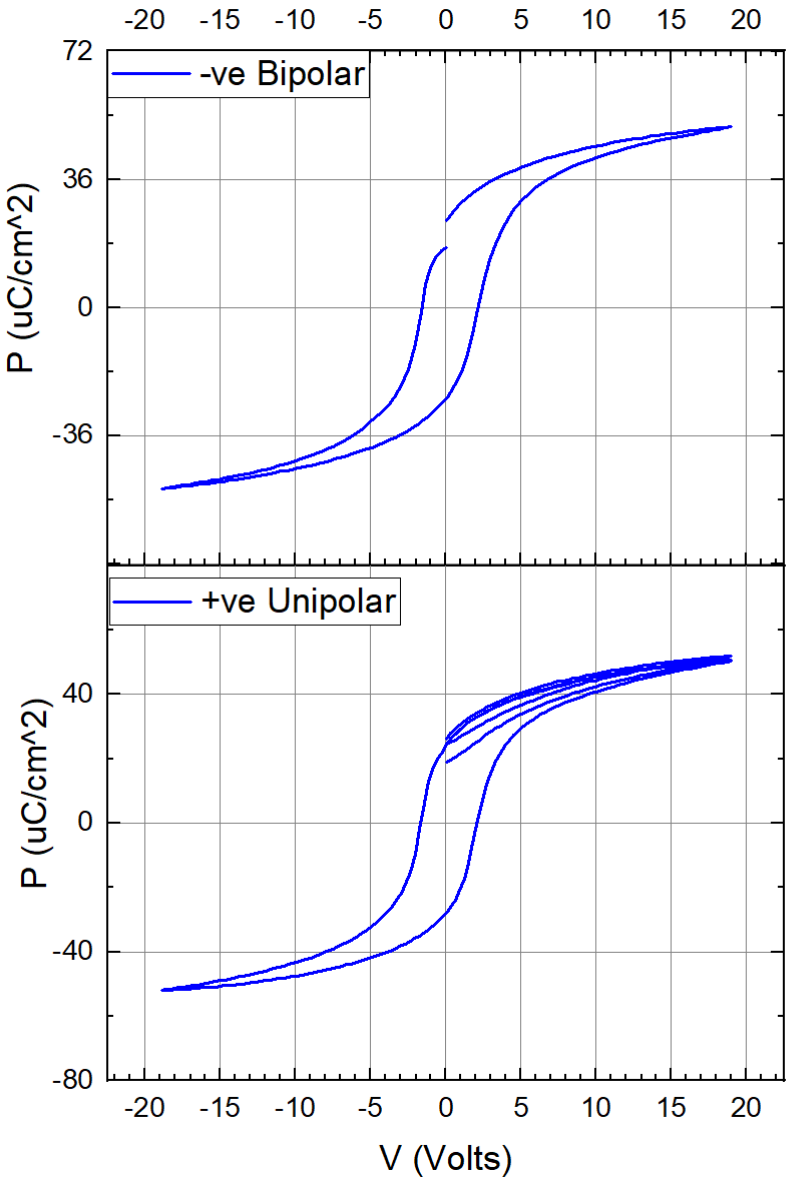

Fig. 9 a) Bipolar and unipolar polarization curves for Sample 1 PZT on CLN Pt (500 °C). b) Sample 2 PZT on AJA Pt (800 °C). c) Sample 3 PZT on AJA Pt (700 °C). d) Sample 4 PZT on AJA Pt (600 °C). e) Sample 5 PZT on AJA Pt (500 °C). f) Sample 6 PZT on AJA Pt (600 °C). g) Sample 7 PZT on AJA Pt (600 °C). h) Sample 8 PZT on AJA Pt (600 °C) (continued).

e)

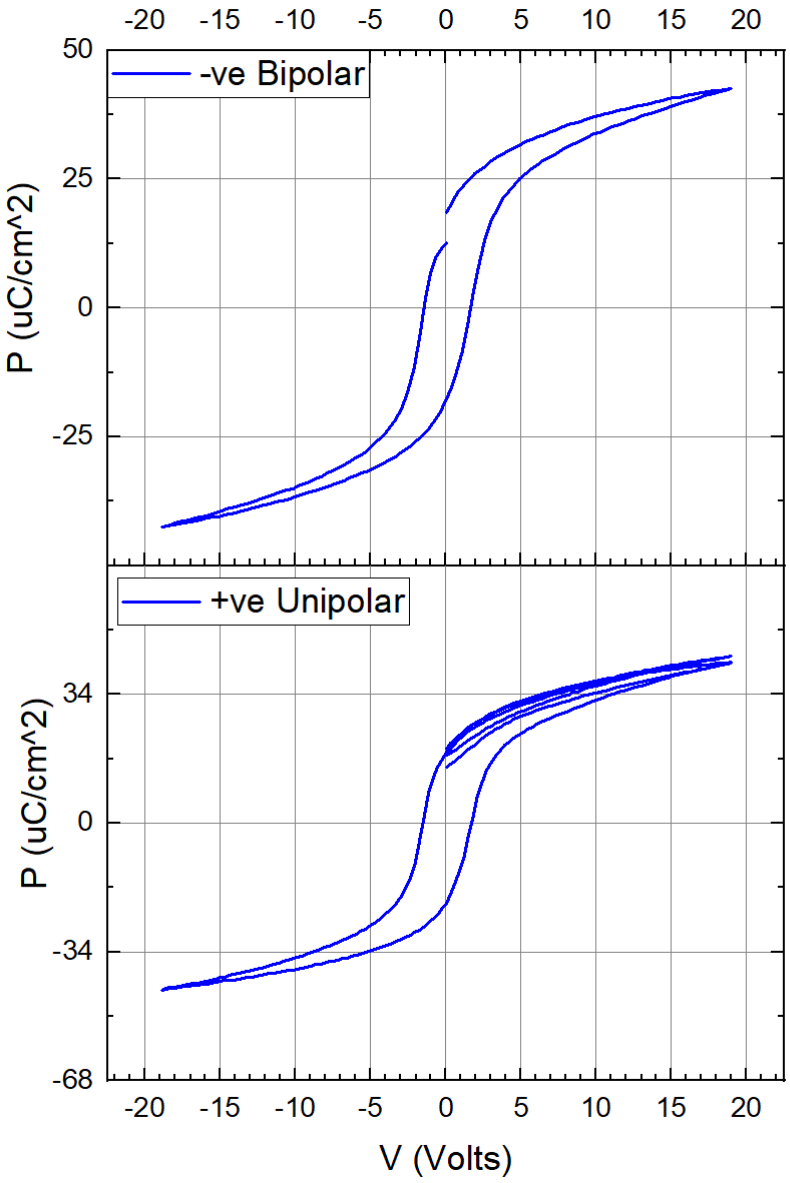

Fig. 9 a) Bipolar and unipolar polarization curves for Sample 1 PZT on CLN Pt (500 °C). b) Sample 2 PZT on AJA Pt (800 °C). c) Sample 3 PZT on AJA Pt (700 °C). d) Sample 4 PZT on AJA Pt (600 °C). e) Sample 5 PZT on AJA Pt (500 °C). f) Sample 6 PZT on AJA Pt (600 °C). g) Sample 7 PZT on AJA Pt (600 °C). h) Sample 8 PZT on AJA Pt (600 °C) (continued).

f)

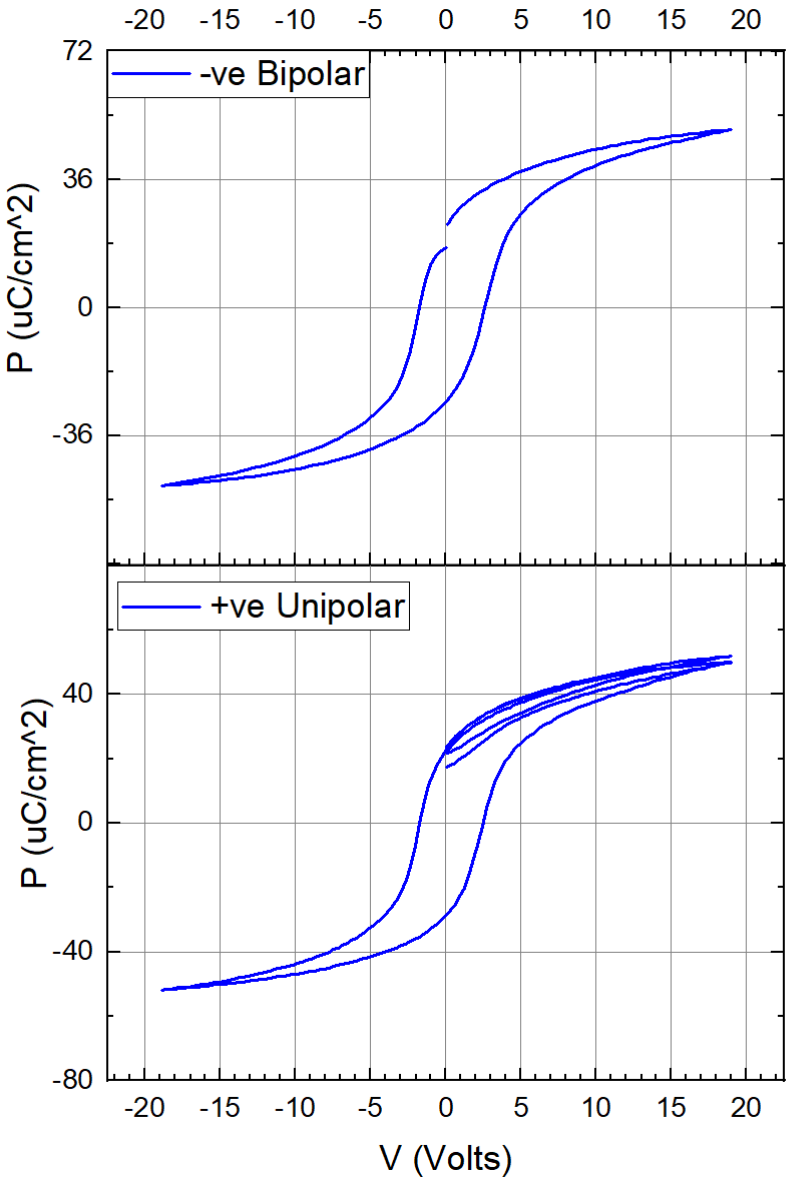

Fig. 9 a) Bipolar and unipolar polarization curves for Sample 1 PZT on CLN Pt (500 °C). b) Sample 2 PZT on AJA Pt (800 °C). c) Sample 3 PZT on AJA Pt (700 °C). d) Sample 4 PZT on AJA Pt (600 °C). e) Sample 5 PZT on AJA Pt (500 °C). f) Sample 6 PZT on AJA Pt (600 °C). g) Sample 7 PZT on AJA Pt (600 °C). h) Sample 8 PZT on AJA Pt (600 °C) (continued).

g)

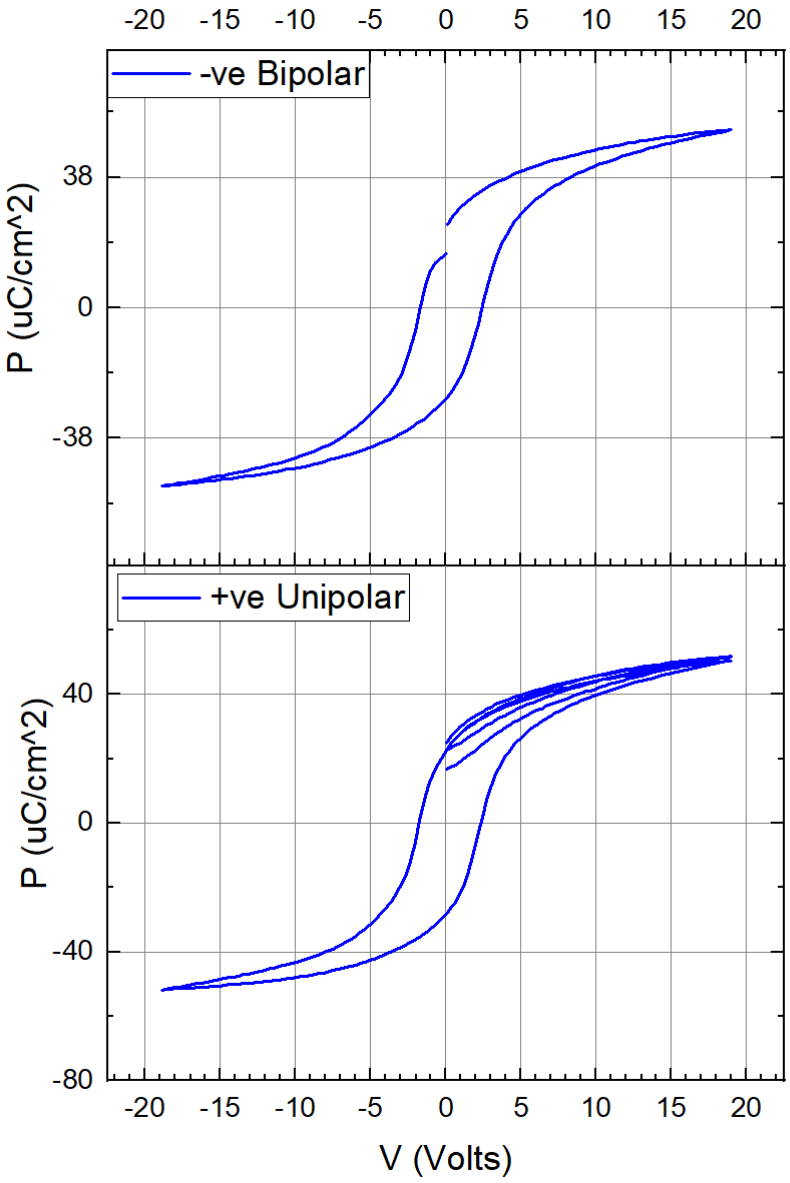

Fig. 9 a) Bipolar and unipolar polarization curves for Sample 1 PZT on CLN Pt (500 °C). b) Sample 2 PZT on AJA Pt (800 °C). c) Sample 3 PZT on AJA Pt (700 °C). d) Sample 4 PZT on AJA Pt (600 °C). e) Sample 5 PZT on AJA Pt (500 °C). f) Sample 6 PZT on AJA Pt (600 °C). g) Sample 7 PZT on AJA Pt (600 °C). h) Sample 8 PZT on AJA Pt (600 °C) (continued).

h)

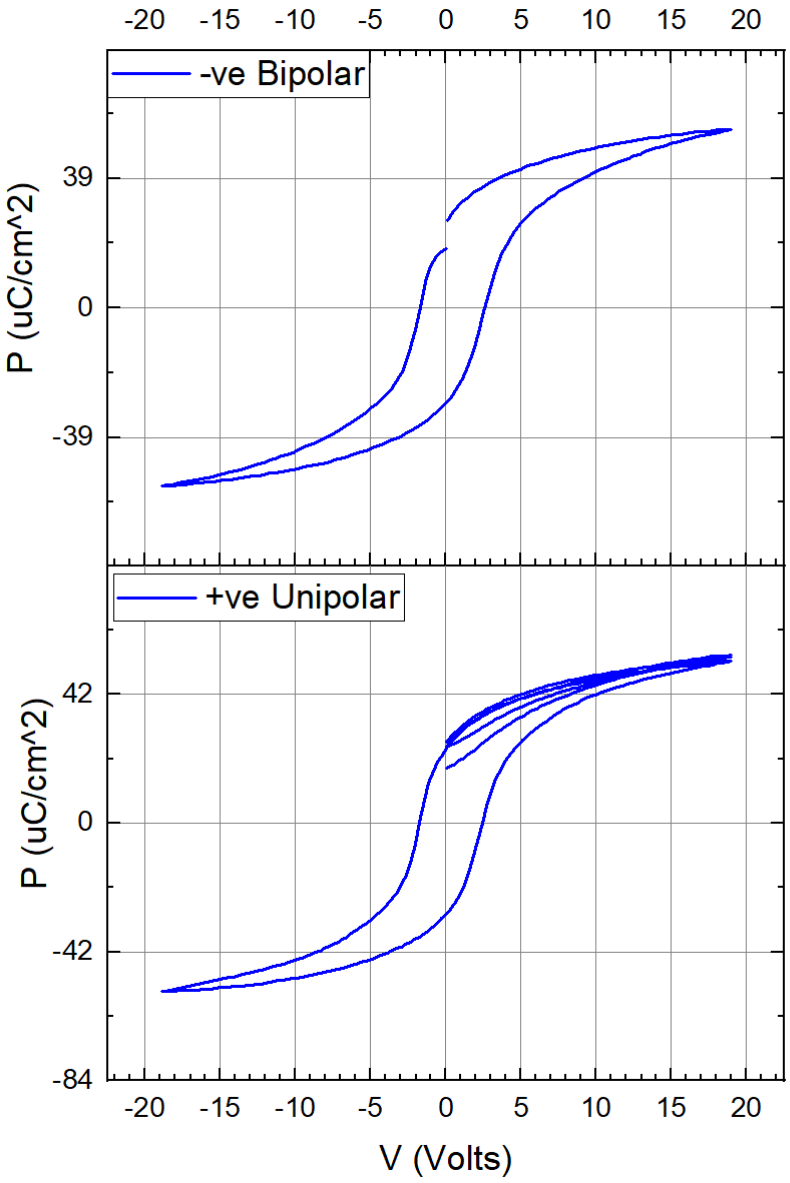

Fig. 9 a) Bipolar and unipolar polarization curves for Sample 1 PZT on CLN Pt (500 °C). b) Sample 2 PZT on AJA Pt (800 °C). c) Sample 3 PZT on AJA Pt (700 °C). d) Sample 4 PZT on AJA Pt (600 °C). e) Sample 5 PZT on AJA Pt (500 °C). f) Sample 6 PZT on AJA Pt (600 °C). g) Sample 7 PZT on AJA Pt (600 °C). h) Sample 8 PZT on AJA Pt (600 °C) (continued).

4. Summary and Conclusion

The set of experiments performed in this report has shown that Pt sputtered in the AJA is a viable alternative to CLN Pt, which provides ARL with a reliable backup source for Pt bottom electrodes. The 500 °C AJA Pt bottom electrode is the best match to the CLN. An additional study that includes post-patterning anneal is required to determine the feasibility and reliability of using AJA Pt as a top electrode for ARL PZT, focused on film adhesion and sheet resistance versus temperature. The 500 °C AJA Pt is comparable in physical characteristics to the CLN Pt. Since stress and other factors may be at play, some other things can be tried. Better stress matching at the higher temperatures is one option. The experimental path forward also has the goal of better temperature control through idling and ramping manipulation. Based on the electrical measurements, the PZT for AJA Pt at 500–800 °C meets the required PZT performance, and stress and other factors can be explored to optimize Pt texture away from 500 °C. The tradeoff is that the AJA process is slow (hours) compared to CLN Pt (minutes). Since much of the extra process time occurs during the temperature ramps up to process temperature and cooldown after deposition, it may be beneficial to explore ways to optimize those or coordinate with the manufacturer to remove this problem as it is not intrinsic to the capability to produce the film quality of the platinum.

5. References

1. Frederic N, editor. MEMS sensors and resonators. Special Issue. Sensors. 2019;19(16). https://www.mdpi.com/journal/sensors/special_issues/MEMS_SENSORS.

2. Carty E, Fitzgerald P, McDaid P. The fundamentals of analog devices' revolutionary MEMS switch technology. Analog Devices. 2016;TA15236-.1-11/16. https://www.analog.com/en/technical-articles/fundamentals-adi-revolutionary-mems-switch-technology.html#.

3. Jære L. Have you heard about PiezoMEMS technology? Norwegian Sci-Tech News - Research News from NTNU and SINTEF. 2018 Sep 19. https://norwegianscitechnews.com/2018/09/have-you-heard-about-piezomems-technology/.

4. Sintef MiNaLab. PiezoMEMS Applications. c2021 [accessed 2021 Mar 4]. https://www.piezomems.com/piezomems-applications/.

5. Basu J, Bhattacharyya TK. Microelectromechanical resonators for radio frequency communication applications. Microsys Tech. 2011;17, article 1557. https://doi.org/10.1007/s00542-011-1332-9.

6. Chen Z, Kan X, Yuan Q, Wang T, Yang J, Yang F. A switchable high-performance RF-MEMS resonator with flexible frequency generations. Sci Rep. 2020;10, article 4795. https://doi.org/10.1038/s41598-020-61744-2.

7. Xu L, Wang S, Jiang Z, Wei X. Programmable synchronization enhanced MEMS resonant accelerometer. Microsys Nanoeng. 2020;6, article 63. https://doi.org/10.1038/s41378-020-0170-2.

8. Murphy C. Choosing the most suitable MEMS accelerometer for your application—part 1. Analog Dialog. 2017 Oct; 51-10. https://www.analog.com/en/analog-dialogue/articles/choosing-the-most-suitable-mems-accelerometer-for-your-application-part-1.html.

9. Benoit RR, Rudy RQ, Pulskamp JS, Polcawich RG, Bedair SS. Advances in piezoelectric PZT-based RF MEMS components and systems. J. Micromech. Microeng. 2017;27(8):083002. https://iopscience.iop.org/article/10.1088/1361-6439/aa710b/meta.

10. Smith GL, Pulskamp JS, Sanchez LM, Potrepka DM, Proie RM, Ivanov TG, Rudy RQ, Nothwang WD, Bedair SS, Meyer CD, Polcawich RG, PZT-based piezoelectric MEMS technology, J Am Ceram Soc. 2012;95(6):1777–1792. DOI: 10.1111/j.1551-2916.2012.05155.x.

11. Potrepka DM, Benoit RR, Rudy RQ, Pulskamp JS, Fox GR, Cheng CY, Trolier-McKinstry S. Effect of titanium (Ti)-seed and in vacuo process flow on sputtered lead zirconate titanate thin films. CCDC Army Research Laboratory; 2019 Sep. Report No.: ARL-MR-1007.

12. Fox GR, Potrepka DM, Polcawich RG. Dependence of {111}-textured Pt electrode properties on TiO_2 seed layers formed by thermal oxidation, J Mater Sci Mater Electron. 2018;29:412–426. DOI 10.1007/s10854-017-7930-2.

13. Strnad NA, Hanrahan BM, Potrepka DM, Pulskamp JS, Phaneuf RJ, Polcawich RG. Growth of thin film ferroelectric PZT, PHT, and antiferroelectric PHO from atomic layer deposition precursors, J Am Ceram Soc. 2020;00:1–13. DOI: 10.1111/jace.17521.

14 Potrepka DM, Rivas M, Yu H, Aindow M, Fox GR, Polcawich RG. Effect of IrO_2/Pt, IrO_2, and Pt bottom electrodes on the structure and electrical properties of PZT based piezoelectric microelectromechanical system devices. J Mater Sci: Mater Electron. 2018;29:11367–11377. https://doi.org/10.1007/s10854-018-9224-8.

15. Benoit RR, Rudy RQ, Pulskamp JS, Polcawich RG. Piezoelectric RF MEMS switches on Si-on-Sapphire substrates. J Microelectromech Sys. 2020 Oct;29(5):1087–1090. DOI: 10.1109/JMEMS.2020.3008201.

16. Puder JM, Pulskamp JS, Rudy RQ, Polcawich RG. A general analytical formulation for the motional parameters of piezoelectric MEMS resonators. IEEE Trans Ultrason Ferroelectr Freq Control. 2018 Mar;65(3 Special Issue), 476–488. DOI: 10.1109/TUFFC.2018.2793099.

17. Tellers MC, Pulskamp JS, Bedair SS, Rudy RQ, Kierzewski IM, Polcawich RG, Bergbreiter SE. Characterization of a piezoelectric MEMS actuator surface toward motion-enabled reconfigurable RF circuits. J Micromech Microeng. 2018 Mar;28(3):035001. DOI: 10.1088/1361-6439/aaa218.

18. Benoit RR, Rudy RQ, Pulskamp JS, Polcawich RG, Bedair SS. Advances in piezoelectric PZT-based RF MEMS components and systems. J Micromech Microeng. 2017 Aug;27(8), article 083002. DOI: 10.1088/1361-6439/aa710b.

19. Rahman MS, Garcia CD, Bhalla A, Guo R. Optical characterization of ferroelectric PZT thin films by variable angle spectroscopic ellipsometry. Proc. SPIE 9200, Photonic Fiber and Crystal Devices: Advances in Materials and Innovations in Device Applications VIII, 2014 Sep 5. 92000A. doi: 10.1117/12.2064658.

20. Chvostová D, Pajasová L, Železný V. Optical properties of PZT thin films by spectroscopic ellipsometry and optical reflectivity. Phys Stat Sol C. 2008;5(5):1362–1365. DOI: 10.1002/pssc.200777869.

21. Potrepka DM, Rivas M, Yu H, Polcawich RG, Aindow M, Fox GR. Characterization of IrOx sputtering for IrO2 and IrO2/Pt bottom-electrode piezoelectric micro-electro-mechanical systems applications. Thin Solid Films. 2017;638:127–137. DOI: 10.1016/j.tsf.2017.07.024.

Appendix A. Supplementary Tables for Evatec Clusterline 200 Processes

A.1 Ti Chamber Preparation

Table A-1 Ti Precondition 1800-s flow

Flow	1RGP_Ti Pre Condition_1000W_30sccm_1800s
O⊙	Start
A1	Align0
P1	Ti_PCM_1000W_30sccm_1800s
X⊗	End

Table A-2 Ti Precondition 1800-s sequence

Sequence	Ti_PCM_1000W_30sccm_1800s
Step 1	Pump out
Step 2	Ar 30 sccm, 60 s, (40 °C)
Step 3	1kW, Ar 30 sccm, 1800 s, (40 °C)
Step 4	Pump out

Table A-3 Ti Process Control Monitor (PCM) deposition 27-s flow

Flow	1RGP_Ti_0500W_30sccm_0027s
O⊙	Start
A1	Align0
P1	Ti_PCM_0500W_30sccm_0027s
X⊗	End

Table A-4 Ti PCM deposition 27-s sequence

Sequence	Ti_PCM_0500W_30sccm_0027s
Step 1	Pump out
Step 2	Ar 30sccm, 60s, (40°C)
Step 3	0.5kW, Ar 30sccm, 27s, (40°C)
Step 4	Pump out

Table A-5 Ti preconditioning and PCM results

Substrate	Slot	T (°C)	P (mbar)	Date	Time	Comments
Si	1	40	2.75E-03	11 5 19	745	Pressure ~ 2.75E-03
Si	2	41	2.80E-03	11 5 19	812	2.80-->2.79 E-03 Pressure settles
Si	3	41	2.92E-03	11 5 19	850	2.92-->2.79 E-03 Pressure settles
Si	4	41[a]	3.06E-03	11 5 19	924	3.06-->2.75 E-03 Pressure settles
5kÅ SiO2	5-ARL12481	41	3.03E-03[b]	11 5 19	955	PCM wafer[c]

[a] 43 °C during pumpout
[b] 1.94E-7 mbar during initial pumpout, 2.99E-03 mbar during Gas Stab 60 s
[c] Rs = 56.11 ± 0.86 Ω/sq (Wf ARL-12481)

A.2 Ir Chamber Preparation

Table A-6 Automated temperature ramp flow for PM3

Flow	PM3Tempramp100Cto450C
O⊙	Start
A1	Align0
P3	PM3_TempRamp_100to450c
C0	Cool60s
X⊗	End

Table A-7 Automated temperature ramp sequence for PM3

Function	T (s)
pump & 200C	400
250C	400
300C	300
350C	300
400C	300
pump & 450C	300

Table A-8 Chamber pressure for automated and manual temperature adjustments for PM3

PM	T start (°C)	T end (°C)	
3	100	450	Time
T (°C)	P (mbar)	Date	
100–450	4.68E-07	11 4 19	1150-1300
450	4.97E-07	11 5 19	810
500	Changed Temp	11 5 19	812
500	2.10E-04	11 5 19	824
500	7.20E-05	11 5 19	827
500	2.95E-04	11 5 19	906
500	2.44E-04	11 5 19	927
500	1E-5-8.3E-6	11 5 19	1316
497	8.57E-05	11 5 19	1427

A.3 Lead Zirconate Titanate (PZT) Chamber Preparation

Table A-9 Automated temperature ramp flow for PM6

Flow	PM6_T ramp_100c - 620c
O⊙	Start
A1	Align0
P3	TempRamp_100Cto620C
C0	Cool60s
X⊗	End

Table A-10 Automated temperature ramp sequence for PM6. Seq: TempRamp_100Cto620C

Function	T (s)
pump & 100C	60
100C	600
200C	600
350C	600
300C	600
400C	600
500C	600
620C	600
pump & 620C	60

Table A-11 Chamber pressure (gas flows off = 0 sccm) for automated and manual temperature adjustments for PM6

PM	T start (°C)	T end (°C)	
6	100	620	Time
T (°C)	P (mbar)	Date	
100	2.60E-08	11 4 19	1300
300	2.75E-08	11 4 19	. . .
400	8.80E-08	11 4 19	. . .
500	1.47E-08	11 4 19	. . .
590	1.66E-07	11 4 19	. . .
601	1.75E-07	11 4 19	. . .
600	2.17E-07	11 4 19	1545
620	~8.5E-8	11 5 19	730
620	T Change to 630C	11 5 19	730
630	8.41E-08	11 5 19	812
640	T Change to 640C	11 5 19	815
640	8.73E-08	11 5 19	825
640	9.00E-08	11 5 19	908
639	2.10E-07	11 5 19	1020
640	2.19E-07	11 5 19	1024

Table A-12 PZT power conditioning flow

Flow	PZT_PCOND2000
O⊙	Start
A1	150 Flat (identical to Align0)
P6	P_Cond2000W
C0	Cool60s
X⊗	End

Table A-13 PZT power conditioning sequence

Sequence	P_Cond2000W
Step 1	Pump 60s (Cs/Csh=550/900)
Step 2	60s 80sccmGas1Ar (750/900)
Step 3	P_Cond_Fire 80sccmAr, 500W, 5s (750/900)
Step 4	120s (750/900) 500 W
Step 5	120s (750/900) 1000 W
Step 6	120s (750/900) 1500 W
Step 7	120s (750/900) 2000 W
Step 8	120s (750/900) 2000 W
Step 9	120s (750/900) 1500 W
Step 10	120s (750/900) 1000 W
Step 11	120s (750/900) 500 W
Step 12	Pump 60s (Cs/Csh=550/900)

Table A-14 Ar conditioning flow

Flow	PZT_Ar_cond
O⊙	Start
A1	150 Flat (identical to Align0)
P6	Ar_Cond
C0	Cool60s
X⊗	End

Table A-15 Ar conditioning sequence

Sequence	Ar_Cond
Step 1	Pump 60s (Cs/Csh=750/900)
Step 2	Gas1 80sccm 60s (750/900)
Step 3	P_Cond_Fire 80sccmAr, 500W, 5s (750/900)
Step 4	2000W (750/900) 120s, 20 sccm Ar
Step 5	2000W (750/900) 120s, 40 sccm Ar
Step 6	2000W (750/900) 120s, 50 sccm Ar
Step 7	2000W (750/900) 120s, 60 sccm Ar
Step 8	2000W (750/900) 120s, 80 sccm Ar
Step 9	2000W (750/900) 120s, 100 sccm Ar
Step 10	2000W (750/900) 120s, 150 sccm Ar
Step 11	2000W (750/900) 120s, 200 sccm Ar
Step 12	Pump 60s (Cs/Csh=750/900)

Table A-16 Chamber observations after Conditioning in PM6. JobID: PM6_PCOND_ArCond_dmp

Substrate	Slot-ID	T (°C)	P (mbar)	Date	Time	Flow
PZT Dummy	1-6371	640.0	1.35E-05	11 5 19	1035	PZT_PCOND2000
PZT Dummy	2-6408	640.0	1.30E-05	11 5 19	1053	PZT_Ar_cond

A.4 Processes for Pt Reheat, Ti Seed Layer, and PZT

Table A-17 Flow for reheat AJA Pt in the Ir chamber, Ti seed layer deposition, and PZT deposition

Flow	DMP_P3AJAPtRebake_PZT_0.5um
O⊙	Start
A1	Align0
P3	PM3_Pdown_500C_600s (Step=PM3_TEMP500C_600s)
P1	Ti_PCM_0250W_30sccm_3sec
P6	1CC_PZTNucVolCombined_2kW_600s_GM_550-900
C0	Cool 60s
X⊗	End

Table A-18 Align0 aligner sequence

Step (Name)	1: 150 Flat
Descriptions	Setpoints
Fiducial angle (deg)	0
Fiducial type	#Flat
Wafer shape	#Round
Wafer size	#Round150mm

Table A-19 PM3(Ir) step for the Pt reheat sequence: PM3_Pdown_500C_600s (used because PM4(Pt) was out of service)

Step	Setting	Description
1	0	Chuckgas Flow (sccm)
2	0	Chuckgas Pressure (mbar)
3	#Don'tChange	Chuck Temp Control Mode
4	500	Chuck Temperature (°C)
5	10	Chuck Heater Power Ratio
6	#Power	DC Generator Control Mode
7	0	DC Generator Current (A)
8	0	DC Generator Power (W)
9	0	DC Generator Ramp Time (s)
10	1.0	DC Generator Shield Life Counting
11	1.0	DC Generator Target Life Counting
12	0	DC Generator Voltage (V)
13	0	DC Generator hard-arc supervision
14	0	DC Generator micro-arc supervision
15	0	Pressure (mbar)
16	#Time	Process end condition
17	600.0	Process Time (s)
18	False	Used for Restart
19	#DCVoltage	RF-Bias control mode
20	0	RF-Chuck Selfbias Voltage (V)
21	0	RF-Bias Load Power (W)
22	0	RF-Bias Ramp Time (s)
23	0	RF-Bias Reflective Power (W)
24	False	HV-iso Throttled
25	0	Ar (sccm)
26	0	N2 (sccm)
27	0	O2 (sccm)
28	0	DC-Chopper frequency (kHz)
29	400.0	DC-Chopper pulse off time (ns)

Table A-20 PM1 Ti seed layer steps in the sequence: PM1 Ti sequence = Ti_PCM_0250W_30sccm_3sec

Step (Name)	1: Pumpdown_Ti_040c	2: GasOn_Ti	3: Ti_0250W_30sccm_3s	4: PumpClean_Ti
Descriptions	Setpoints			
Chuckgas flow (sccm)	0.0	5.0	5.0	0.0
Chuckgas pressure (mbar)	0.0	8.0	8.0	0.0
Chuck temp-control mode	#Setpoint	#Don'tChange	#Don'tChange	#Don'tChange
Chuck temperature (degC)	40.0	40.0	40.0	40.0
Chuck heater power ratio	10	10	10	10
DC-Generator control mode	#Power	#Power	#Power	#Power
DC-Generator current (A)	0.0	0.0	0.0	0.0
DC-Generator power (W)	0.0	0.0	250.0	0.0
DC-Generator ramp time (s)	0.0	0.0	0.0	0.0
DC Generator Shield-life counting rate	1.0	1.0	1.0	1.0
DC-Generator Target-life counting rate	1.0	1.0	1.0	1.0
DC-Generator voltage (V)	0.0	0.0	0.0	0.0
DC-Generator hard arc supervision	0	0	0	0
DC-Generator micro arc supervision	0	0	0	0
Pressure (mbar)	5.0E-06	5.0E-03	5.0E-03	5.0E-06
Process-end condition	#Time	#Time	#Time	#Time
Process time (s)	30.0	60.0	3.0	30.0
Used for restart	false	false	false	false
RF-Bias control mode	#DCVoltage	#DCVoltage	#DCVoltage	#DCVoltage
RF-Chuck selfbias voltage. (V)	0.0	0.0	0.0	0.0
RF-Bias load-power (W)	0.0	0.0	0.0	0.0
RF-Bias ramp tim. (s)	0.0	0.0	0.0	0.0
RF-Bias refl.-power (W)	0.0	0.0	0.0	0.0
HV-iso throttled	false	false	false	false
_Ar (sccm)	0.0	30.0	30.0	0.0
_N2 (sccm)	0.0	0.0	0.0	0.0
_O2 (sccm)	0.0	0.0	0.0	0.0
DC-Chopper frequency. (kHz)	0.0	0.0	0.0	0.0
DC-Chopper puls off time (ns)	400.0	400.0	400.0	400.0

Table A-21 PZT sequence

Sequence	1CC_PZTNucVolCombined_2kW_600s_GM_550-900
Step 1	P_Cond_Pump_550
Step 2	Gas_Stab_60s_550
Step 3	P_Cond_Fire_550_900
Step 4	PZT Nucleate_2kW_30s_080Ar_5BG
Step 5	PZT_2kW_5s_56Ar_GM_550-900
Step 6	PZT_2kW_5s_4O2_GM_550-900_loopto5
Step 7	P_Cond_Pump_550

Table A-22 PZT pumpdown and gas stabilization steps

Step	1: Pumpdown	2: Gas 60 s
Chuckgas flow (sccm)	0.0	0.0
Chuckgas pressure. (mbar)	0.0	0.0
Chuckgas regulation mode	#Pressure	#Pressure
Chuck temp-control mode	#Don'tChange	#Don'tChange
Chuck temperature (degC)	610.0	610.0
Chuck heater power ratio	20	20
Proc.gas1 flow setpoint. (Ar) (sccm)	0.0	80.0
Proc.gas2 flow setpoint (?) (sccm)	0.0	0.0
Proc.gas3 flow setpoint (O2) (sccm)	0.0	0.0
Matching series capacitor (steps)	550.0	550.0
Matching shunt capacitor (steps)	900.0	900.0
PhaseShifterSetpoint (Deg)	0.0	0.0
Pressure (mbar)	5.0E-06	0.0
Process-end condition.	#Pressure	#Time
Process time. (s)	60.0	60.0
Loop times	0	0
Loop to step	0	0
Used for restart.	false	false
RF-Chuck selfbias voltage. (V)	0.0	0.0
RF-Bias load-power (W)	0.0	0.0
RF-Bias ramp time (s)	0.0	0.0
RF-Bias refl.-power (W)	0.0	0.0
RF-Sputter selfbias voltage (V)	0.0	0.0
RF-Sputter load-power (W)	0.0	0.0
RF-Sputter ramp time (s)	0.0	0.0
RF-Sputter refl.-power (W)	0.0	0.0
RF-Sputter matching mode	#Automatic	#Automatic
RF-Sputter series capacitor (steps)	0.0	0.0
RF-Sputter shunt capacitor (steps)	0.0	0.0

Table A-23 PZT process steps

Step	3: Fire Plasma	4: PZT Nucleate	5: PZT 5s Ar	6: PZT 5s Ar O_2 loop to 5
Chuckgas flow. (sccm)	0.0	0.0	0.0	0.0
Chuckgas pressure (mbar)	7.0	6.5	6.5	6.5
Chuckgas regulation mode.	#Pressure	#Pressure	#Pressure	#Pressure
Chuck temp-control mode.	#Don'tChange	#Don'tChange	#Don'tChange	#Don'tChange
Chuck temperature. (degC)	610.0	610.0	610.0	610.0
Chuck heater power ratio	20	20	20	20
Proc.gas1 flow setpoint. (Ar) (sccm)	80.0	80.0	56.0	54.0
Proc.gas2 flow setpoint. (sccm)	0.0	0.0	0.0	0.0
Proc.gas3 flow setpoint (O_2) (sccm)	0.0	0.0	0.0	4.0
Matching series capacitor (steps)	550.0	550.0	550.0	550.0
Matching shunt capacitor (steps)	900.0	900.0	900.0	900.0
PhaseShifterSetpoint (Deg)	0.0	0.0	0.0	0.0
Pressure (mbar)	0.0	0.0	0.0	0.0
Process-end condition.	#Time	#Time	#Time	#Time
Process time (s)	5.0	60.0	60.0	5.0
Loop times	0	0	0	80
Loop to step	0	0	0	5
Used for restart	false	false	false	false
RF-Chuck selfbias voltage (V)	0.0	0.0	0.0	0.0
RF-Bias load-power (W)	0.0	0.0	0.0	0.0
RF-Bias ramp time (s)	0.0	0.0	0.0	0.0
RF-Bias refl.-power (W)	0.0	0.0	0.0	0.0
RF-Sputter selfbias voltage (V)	0.0	0.0	0.0	0.0
RF-Sputter load-power (W)	500.0	2000.0	2000.0	2000.0
RF-Sputter ramp time (s)	0.0	0.0	0.0	0.0
RF-Sputter refl.-power (W)	0.0	0.0	0.0	0.0
RF-Sputter matching mode	#Automatic	#Automatic	#Automatic	#Automatic
RF-Sputter series capacitor (steps)	0.0	0.0	0.0	0.0
RF-Sputter shunt capacitor (steps)	0.0	0.0	0.0	0.0

Table A-24 Cooler sequence

Step (Name)	1: Cool60s
Descriptions	Setpoints
Process time (s)	60.0
Used for restart	false

Table A-25 Tolerances for the Ti and Ir chambers, PM1 and PM3, respectively

Descriptions	Setpoint	±Soft Tolerance	±Hard Tolerance	Min	Max	Units
Chuckgas flow (sccm)	0.0	0.0	0.0	0.0	20.0	sccm
Chuckgas pressure (mbar)	0.0	0.0	0.0	0.0	113.4	mbar
Chuck temp-control mode	#Don'tChange	. . .	. . .	. . .	. . .	. . .
Chuck temperature (degC)	500.0	20.0	50.0	0.0	600.0	degC
Chuck heater power ratio	10	0	0	0	100	10
DC-Generator control mode	#Power	. . .	. . .	. . .	. . .	. . .
DC-Generator current (A)	0.0	0.0	0.0	0.0	40.0	A
DC-Generator power (W)	0.0	0.0	0.0	0.0	10000.0	W
DC-Generator ramp time (s)	0.0	0.0	0.0	0.0	3600.0	s
DC Generator Shield-life counting rate	1.0	0	0	0.1	10.0	
DC-Generator Target-life counting rate	1.0	0	0	0.1	10.0	
DC-Generator voltage (V)	0.0	0.0	0.0	0.0	1500.0	V
DC-Generator hard arc supervision	0	0	0	0	1000000000	
DC-Generator micro arc supervision	0	0	0	0	1000000000	
Pressure (mbar)	0.0	0.0	0.0	0.0	1013.2	mbar
Process-end condition	#Time	. . .	. . .	. . .	. . .	. . .
Process time (s)	600.0	0.0	0.0	0.0	1.0E+06	s
Used for restart	false	. . .	. . .	. . .	. . .	. . .
RF-Bias control mode	#DCVoltage	. . .	. . .	. . .	. . .	. . .
RF-Chuck selfbias voltage (V)	0.0	0.0	0.0	0.0	1000.0	V
RF-Bias load-power (W)	0.0	0.0	0.0	0.0	600.0	W
RF-Bias ramp time (s)	0.0	0.0	0.0	0.0	3600.0	s
RF-Bias refl.-power (W)	0.0	0.0	0.0	0.0	250.0	W
HV-iso throttled	false	. . .	. . .	. . .	. . .	. . .
_Ar (sccm)	0.0	0.0	0.0	0.0	500.0	sccm
_N2 (sccm)	0.0	0.0	0.0	0.0	50.0	sccm
_O2 (sccm)	0.0	0.0	0.0	0.0	100.0	sccm
DC-Chopper frequency (kHz)	0.0	0.0	0.0	0.0	350.0	kHz
DC-Chopper puls off time (ns)	400.0	0	0	400.0	5000.0	ns

Table A-26 Tolerances for the PZT chamber PM6

Description	Setpoint	±Soft Tolerance	±Hard Tolerance	Min	Max	Units
Chuckgas flow (sccm)	0.0	0.0	0.0	0.0	15.4	sccm
Chuckgas pressure (mbar)	0.0	0.0	0.0	0.0	20.0	mbar
Chuckgas regulation mode	#Pressure	. . .	. . .	. . .	. . .	. . .
Chuck temp-control mode	#Disable	. . .	. . .	. . .	. . .	. . .
Chuck temperature (degC)	25.0	20.0	50.0	0.0	850.0	degC
Chuck heater power ratio	10	0	0	10	100	10
Proc.gas1 flow setpoint.(Ar) (sccm)	0.0	0.0	0.0	0.0	200.0	sccm
Proc.gas2 flow setpoint (?) (sccm)	0.0	0.0	0.0	0.0	200.0	sccm
Proc.gas3 flow setpoint (O2) (sccm)	0.0	0.0	0.0	0.0	10.0	sccm
Matching series capacitor (steps)	0	0	0	0	1000	steps
Matching shunt capacitor (steps)	0	0	0	0	1000	steps
PhaseShifterSetpoint (Deg)	0.0	0.0	0.0	0.0	360.0	degC
Pressure (mbar)	0.0	0.0	0.0	0.0	1013.2	mbar
Process-end condition	#Time	. . .	. . .	. . .	. . .	. . .
Process time (s)	10.0	0.0	0.0	0.0	1.0E+06	s
Loop times	0	0	0	. . .	. . .	. . .
Loop to step	0	0	0	. . .	. . .	. . .
Used for restart	. . .	. . .	. . .	. . .	. . .	. . .
RF-Chuck selfbias voltage (V)	0.0	0.0	0.0	-1000.0	1000.0	V
RF-Bias load-power (W)	0.0	0.0	0.0	0.0	600.0	W
RF-Bias ramp time (s)	0.0	0.0	0.0	0.0	3600.0	s
RF-Bias refl.-power (W)	0.0	0.0	0.0	0.0	250.0	W
RF-Sputter selfbias voltage (V)	0.0	0.0	0.0	0.0	1000.0	V
RF-Sputter load-power (W)	0.0	0.0	0.0	0.0	5000.0	W
RF-Sputter ramp time (s)	0.0	0.0	0.0	0.0	3600.0	s
RF-Sputter refl.-power (W)	0.0	0.0	0.0	0.0	1000.0	W
RF-Sputter matching mode	#Manual	. . .	. . .	. . .	. . .	. . .
RF-Sputter series capacitor (steps)	0.0	0.0	0.0	0	1000	steps
RF-Sputter shunt capacitor (steps)	0.0	0.0	0.0	0	1000	steps

Table A-27 Sequence of wafer processing locations as handled by the transfer robot

PM3	PM1	PM6	Arm1	Arm2	Cooler	Boat Slot
1	. . .	. . .	. . .	. . .	. . .	. . .
2	1	. . .	. . .	. . .	. . .	. . .
3	2	1	4	. . .	. . .	. . .
4	3	2		5	1	. . .
5 [a]	4	3	2	. . .	1	. . .
6 [a]	5	3	. . .	4	2	1
. . .	6	4	5	. . .	3	2
. . .	. . .	5		6	4	3
. . .	. . .	6	. . .	. . .	5	4
. . .	. . .	. . .	. . .	. . .	6	5
. . .	. . .	. . .	. . .	. . .	. . .	6

[a]PM3 and PM1 finish up and wait while PM6 is still in process

Table A-28 Process pressures for Pt reheat, Ti seed layer deposition, and PZT deposition

Substrate	Slot-ID	P (mbar)		
		PM3	PM1	PM6
CLN500	1-12139	. . .	. . .	2.65E-03
AJA800	2-12621	(0.5-2)E-04	2.80E-03	2.67E-03
AJA700	3-12774	(0.06-1.71)E-04	2.80E-03	2.65E-03
AJA600	4-12619	3-4E-05	2.77E-03	2.69E-03
AJA500	5-12538	1.04E-04	2.77E-03	2.65E-03
AJA600	6-12434	(1-2)E-04	2.79E-03	2.65E-03
AJA600	7-12438	1.36E-04	2.77E-03	2.65E-03
AJA600	8-12505	7.00E-05	2.84E-03	2.63E-03

Table A-29 Temperatures for Pt reheat, Ti seed layer deposition, and PZT deposition

Process module (PM)	Deposition temperature (°C)
3 – Ir Chamber	500 ± 3
1 – Ti Chamber	40 ± 1
6 – PZT Chamber	640 ± 5

Table A-30 IrO_2 sputtering sequence for top electrode deposition

Sequence	IrOx_1000W_Ar100_O60_0035s
Step 1	Pump out
Step 2	Ar 30sccm, 60s, (40°C)
Step 3	IrOx_1000W_Ar100_O60_35s_450C_CC
Step 4	Pump out

Table A-31 Deposition parameters for 1000 Å top electrode IrO_2 sputtering on Samples 1–8

Quantity	Symbol	Value
Sputtering power	P	1000 W
Current	I	1.6 A
Target cathode voltage	V	637.5±0.5 V
Substrate temperature	T	450 °C
Ultimate pumpdown vacuum	p_{MIN}	(9.5±0.5)E-7 mbar
Pressure during flow	p_{FLOW}	8.7E-3 mbar
Ar flow	Ar Flow	102.0±0.3 sccm
O_2 flow	O_2 Flow	60.5 sccm

Appendix B. Lead Zirconate Titanate (PZT) Film Surface and Atomic Force Microscope (AFM) Images

a.

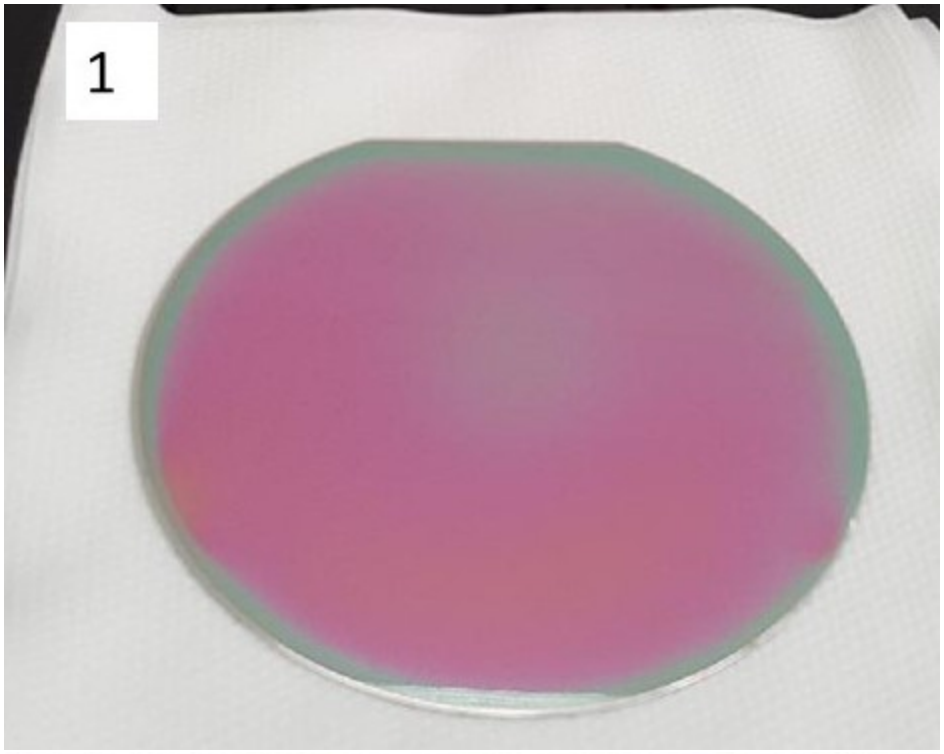

b.

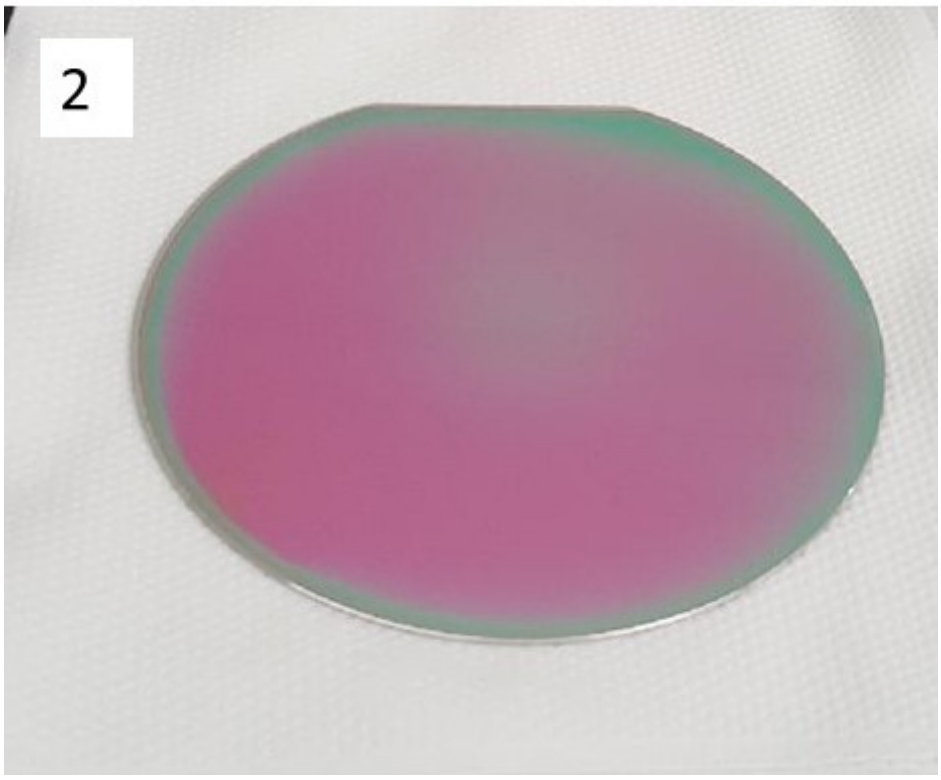

Fig. B-1 Images of wafers after PZT deposition. a) Standard 1000 Å Clusterline Pt deposited at 500 °C (Wafer 1-12139). AJA nominal 800 Å Pt temperature (wafer number): b) 812 °C (2-12621), c) 700 °C (3-12774), d) 600 °C (4-12619), and e) 500 °C (5-12538). AJA nominal 1070 Å Pt temperature (wafer number) f) 600 (6-12434), g) 600 (7-12438), and h) 600 (8-12505).

c.

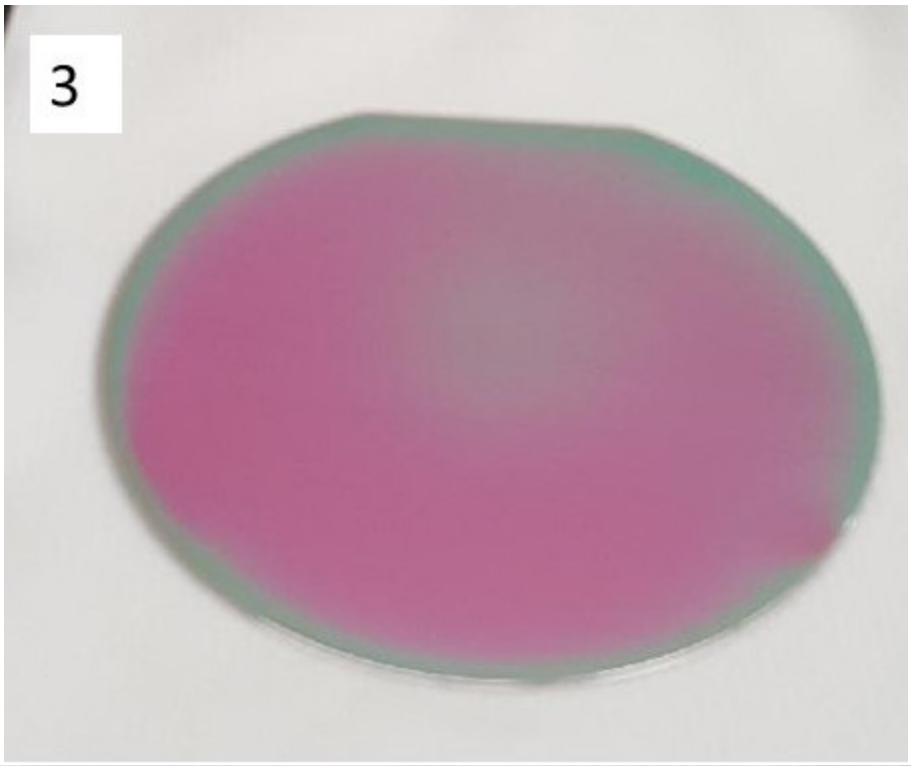

d.

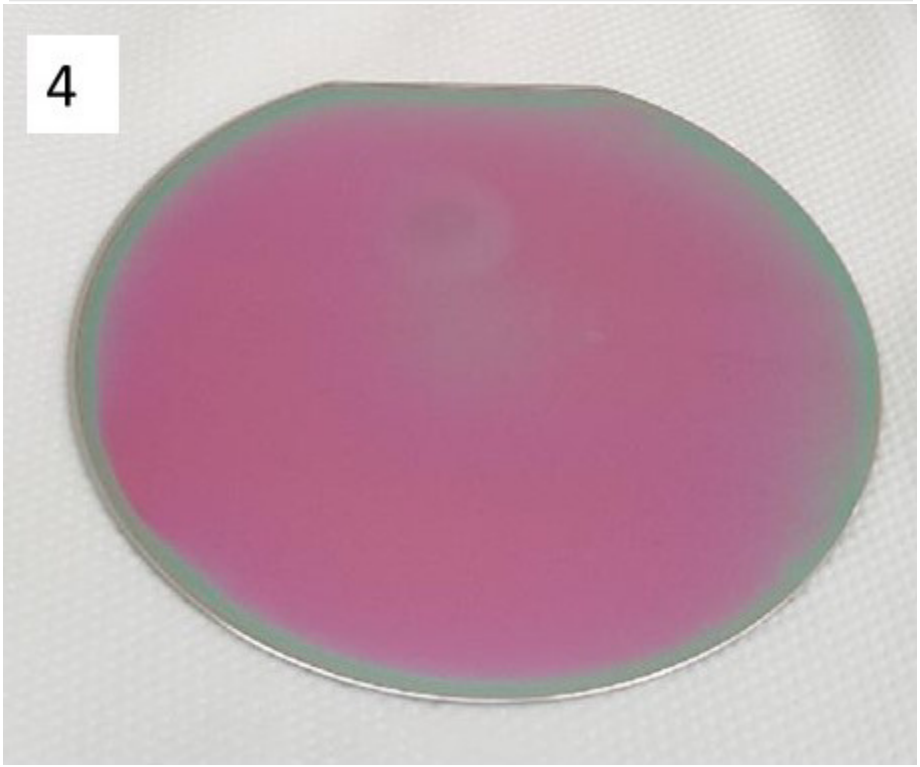

Fig. B-1 Images of wafers after PZT deposition. a) Standard 1000 Å Clusterline Pt deposited at 500 °C (Wafer 1-12139). AJA nominal 800 Å Pt temperature (wafer number): b) 812 °C (2-12621), c) 700 °C (3-12774), d) 600 °C (4-12619), and e) 500 °C (5-12538). AJA nominal 1070 Å Pt temperature (wafer number) f) 600 (6-12434), g) 600 (7-12438), and h) 600 (8-12505) (continued).

e.

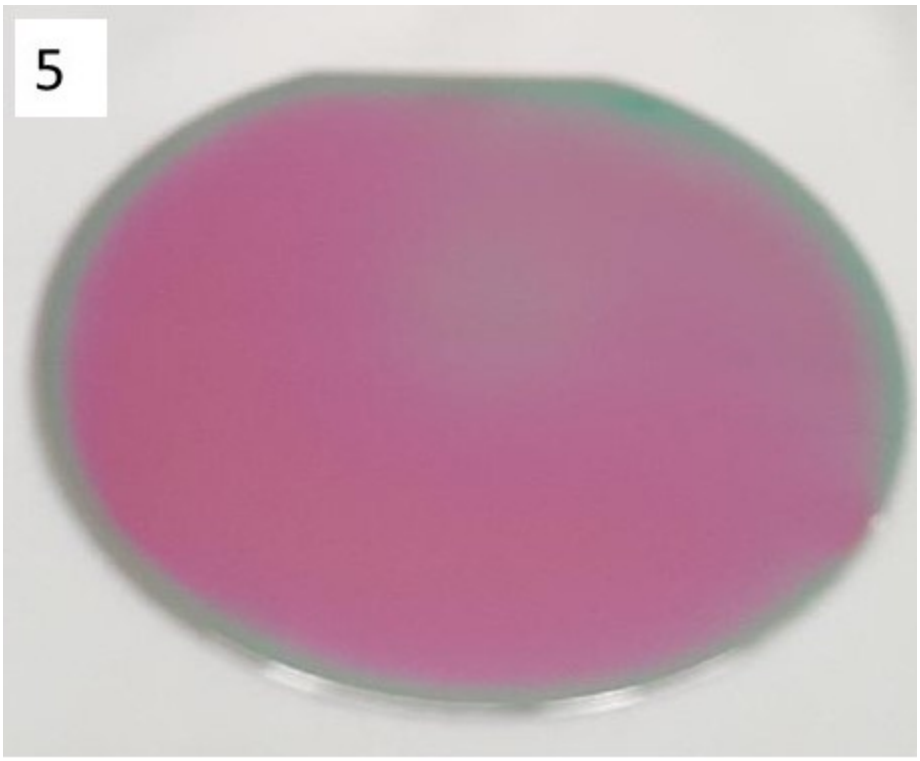

f.

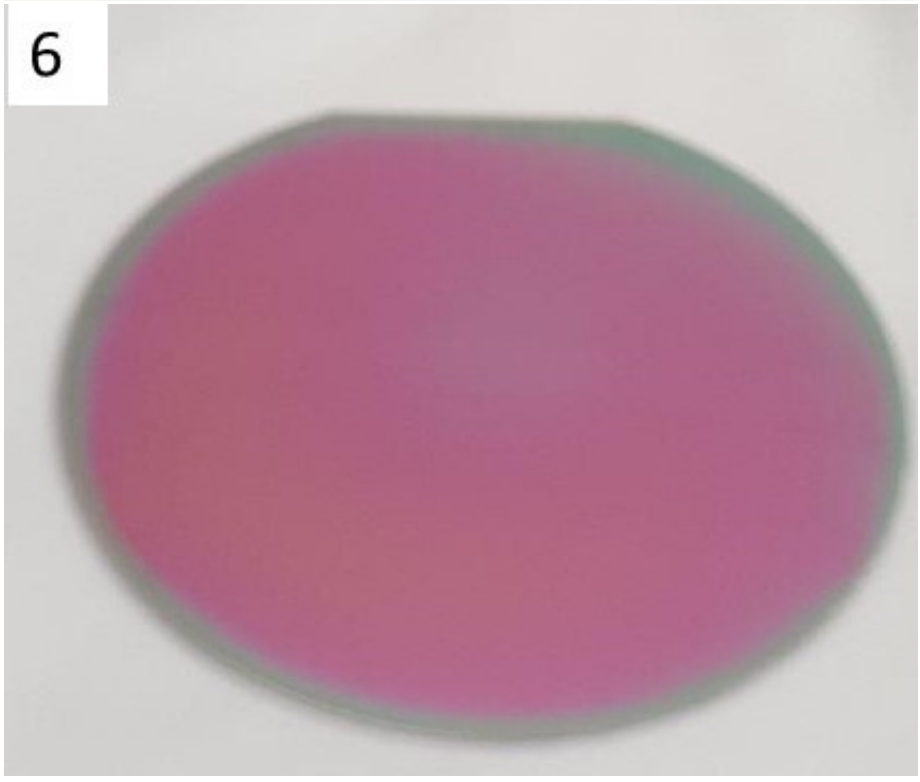

Fig. B-1 Images of wafers after PZT deposition. a) Standard 1000 Å Clusterline Pt deposited at 500 °C (Wafer 1-12139). AJA nominal 800 Å Pt temperature (wafer number): b) 812 °C (2-12621), c) 700 °C (3-12774), d) 600 °C (4-12619), and e) 500 °C (5-12538). AJA nominal 1070 Å Pt temperature (wafer number) f) 600 (6-12434), g) 600 (7-12438), and h) 600 (8-12505) (continued).

g.

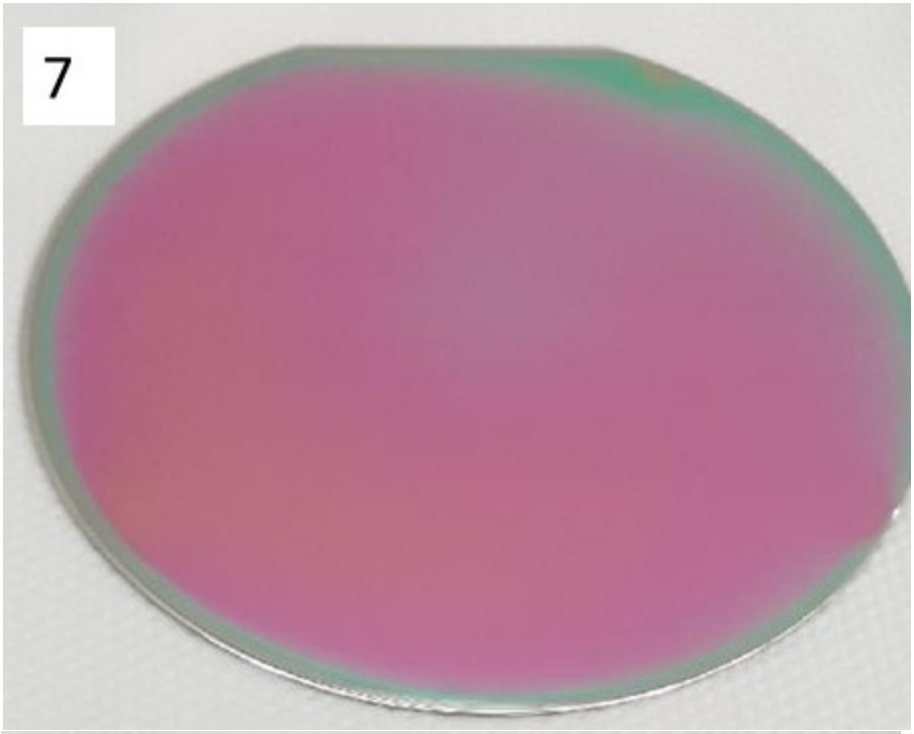

h.

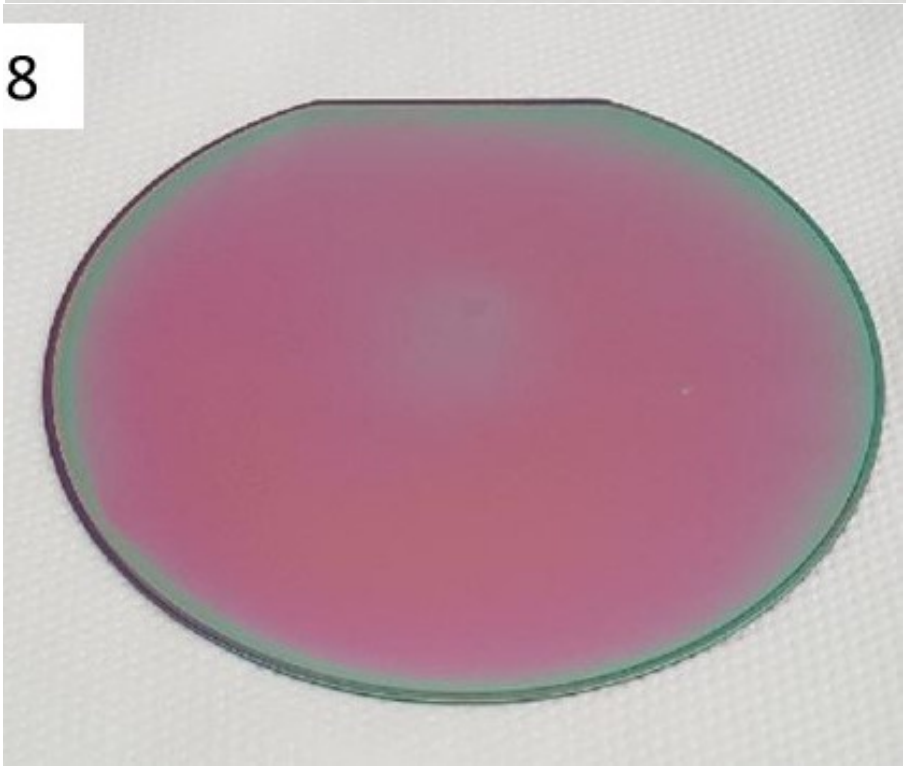

Fig. B-1 Images of wafers after PZT deposition. a) Standard 1000 Å Clusterline Pt deposited at 500 °C (Wafer 1-12139). AJA nominal 800 Å Pt temperature (wafer number): b) 812 °C (2-12621), c) 700 °C (3-12774), d) 600 °C (4-12619), and e) 500 °C (5-12538). AJA nominal 1070 Å Pt temperature (wafer number) f) 600 (6-12434), g) 600 (7-12438), and h) 600 (8-12505) (continued).

a.

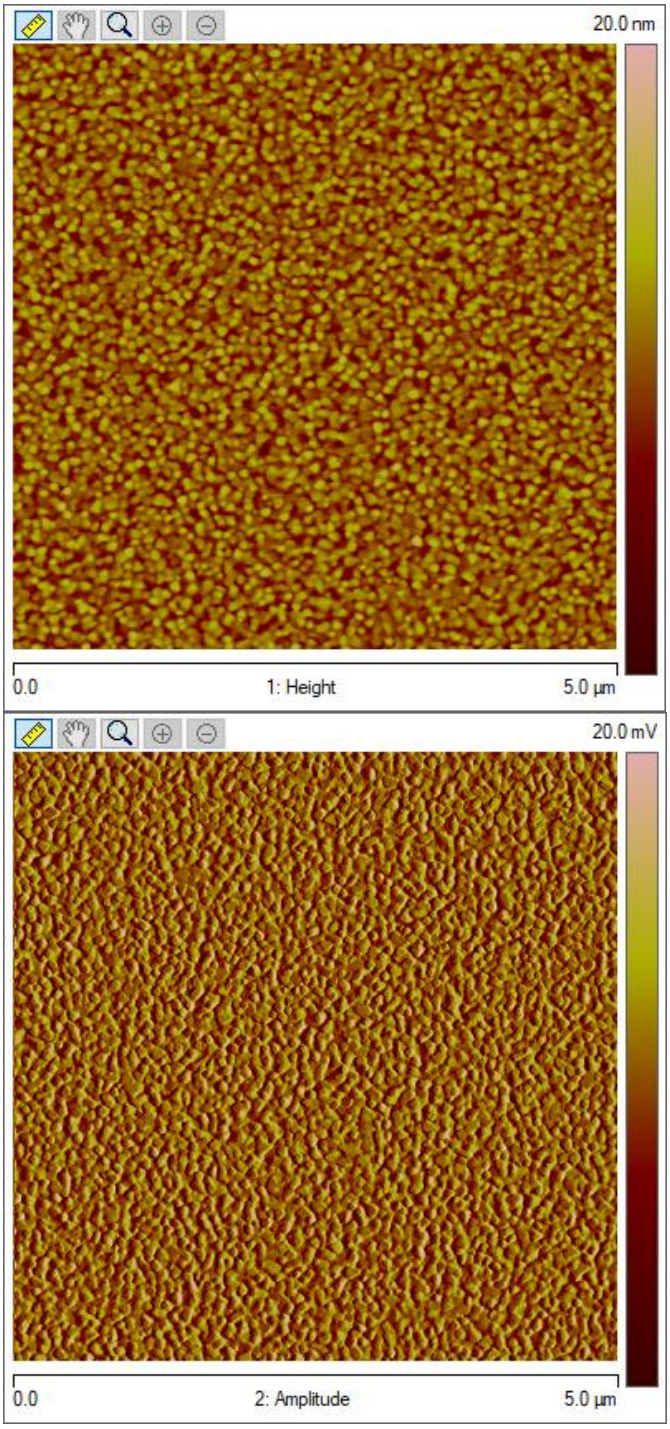

Fig. B-2 AFM height and amplitude images, respectively, at wafer center for a) Standard CLN Pt deposited at 500 °C (Wafer 1-12139), and substrate temperature (wafer number) for AJA Pt deposited at b) 800 °C (2-12621), c) 700 °C (3-12774), d) 600 °C (4-12619), and e) 500 °C (5-12538)

b.

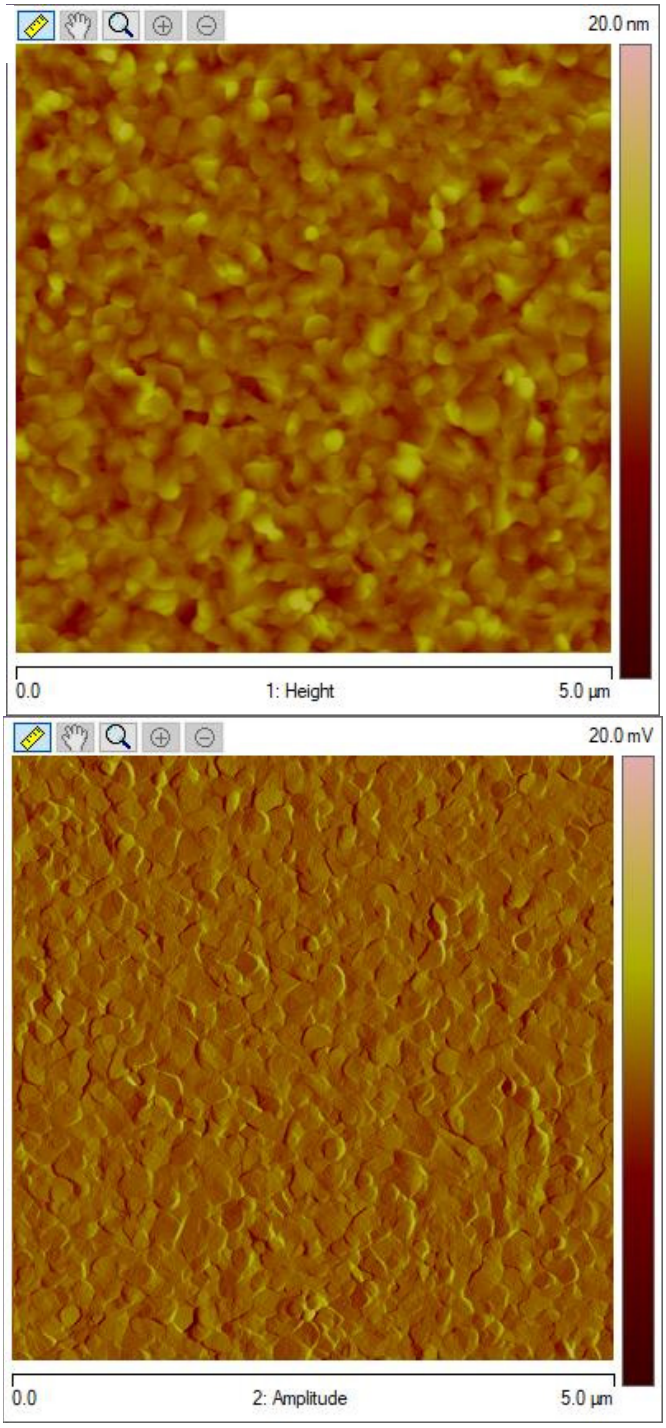

Fig. B-2 AFM height and amplitude images, respectively, at wafer center for a) Standard CLN Pt deposited at 500 °C (Wafer 1-12139) and substrate temperature (wafer number) for AJA Pt deposited at b) 800 °C (2-12621), c) 700 °C (3-12774), d) 600 °C (4-12619), and e) 500 °C (5-12538) (continued).

c.

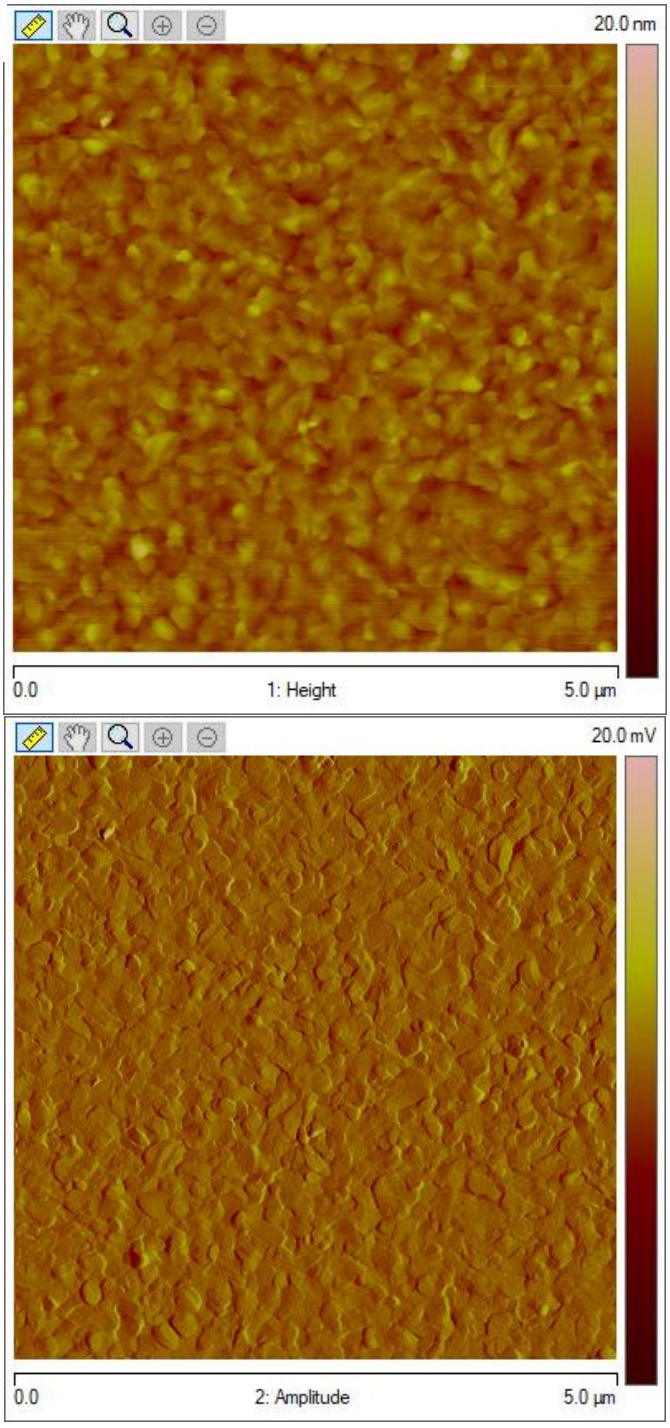

Fig. B-2 AFM height and amplitude images, respectively, at wafer center for a) Standard CLN Pt deposited at 500 °C (Wafer 1-12139), and substrate temperature (wafer number) for AJA Pt deposited at b) 800 °C (2-12621), c) 700 °C (3-12774), d) 600 °C (4-12619), and e) 500 °C (5-12538) (continued).

d.

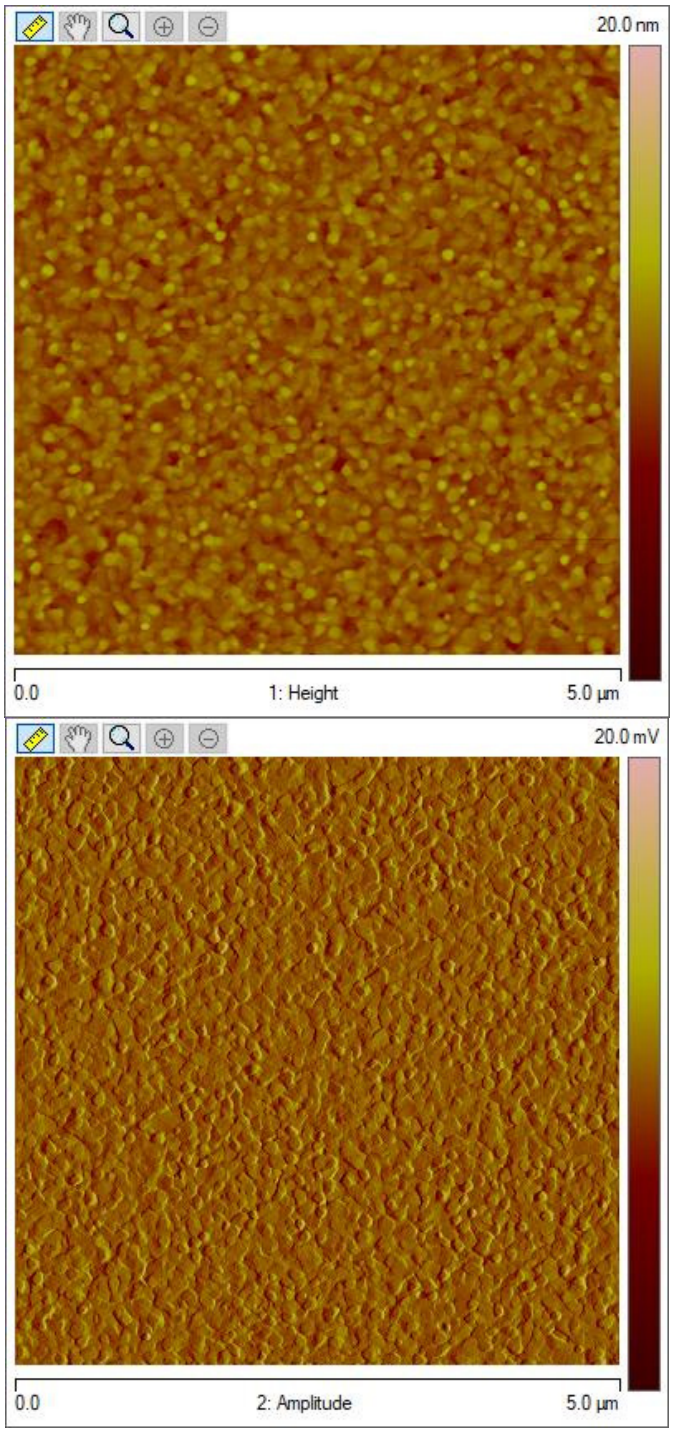

Fig. B-2 AFM height and amplitude images, respectively, at wafer center for a) Standard CLN Pt deposited at 500 °C (Wafer 1-12139), and substrate temperature (wafer number) for AJA Pt deposited at b) 800 °C (2-12621), c) 700 °C (3-12774), d) 600 °C (4-12619), and e) 500 °C (5-12538) (continued).

e.

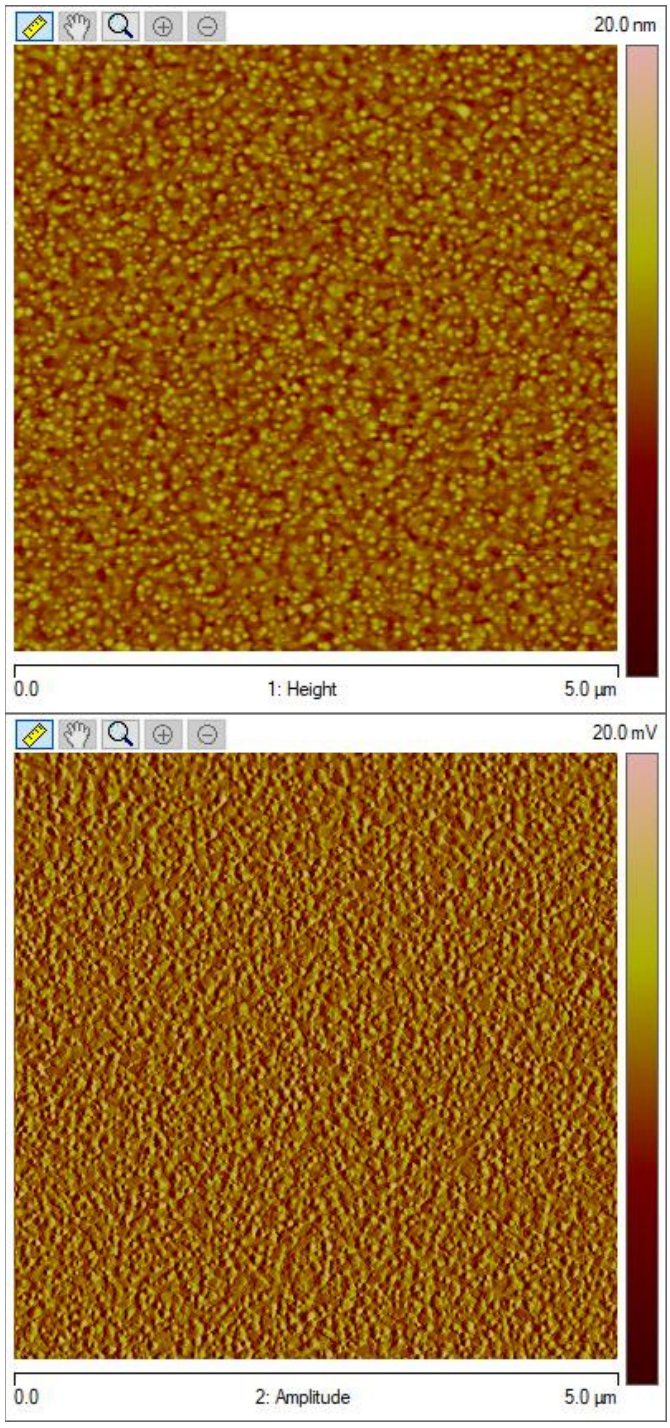

Fig. B-2 AFM height and amplitude images, respectively, at wafer center for a) Standard CLN Pt deposited at 500 °C (Wafer 1-12139), and substrate temperature (wafer number) for AJA Pt deposited at b) 800 °C (2-12621), c) 700 °C (3-12774), d) 600 °C (4-12619), and e) 500 °C (5-12538) (continued).

Appendix C. Electrical Supplemental Data

Table C-1 Breakdown voltages (V_{BD}) corresponding to breakdown electric fields (E_{BD})

Sample ID	V_{BD} (V)	E_{BD} (kV/cm)
1-12139	32.8 ± 7.0	567 ± 121
2-12621	32.2 ± 0.9	554 ± 15
3-12774	36.2 ± 5.1	624 ± 88
4-12619	31.6 ± 2.3	544 ± 40
5-12538	32.0 ± 3.4	553 ± 59
6-12434	46.0 ± 16.4	797 ± 285
7-12438	35.8 ± 2.2	619 ± 38
8-12505	34.4 ± 1.1	596 ± 20
9-12147	32.0 ± 4.5	580 ± 82

List of Symbols, Abbreviations, and Acronyms

AFM	atomic force microscope
AJA	AJA ATC 2200 Co-sputter Deposition System
ARL	Army Research Laboratory
CLN	Evatec Clusterline
DC	direct current
DEVCOM	US Army Combat Capabilities Development Command
FTIR	Fourier transform infrared
FWHM	full width at half maximum
ID	identification
IoT	Internet of Things
MEMS	microelectromechanical system
MIM	metal-insulator-metal capacitor
NatOx	native oxide
PCM	process control monitor
PE	E-field
PM4	Process Module #4
PZT	lead zirconate titanate
Q	quality factor
RC	rocking curve
RF	radio frequency
RMS	root mean square
XRD	X-ray diffraction

Glossary

5G	fifth-generation telecommunication technology
10°–90° θ–2θ scans	X-ray diffraction scan for $(5°,10°) \leq (\theta,2\theta) \leq (45,90)$; a scan where the incident-beam detector angle varies $10° \leq 2\theta \leq 90°$ as the sample detector angle varies $5° \leq 2\theta \leq 45°$.
ε	Greek letter epsilon representing the value of the dielectric constant in dielectric capacitor measurements
Ar Flow	in the context of this report, this refers to the argon that is flowed through the sputtering chamber during the process for the sputtering
AFM	atomic force microscope; atomic force scanning probe microscope (SPM).
E_{BD}	Breakdown (BD) electric field; in a destructive electric field versus increasing current measurement, the measured field at which the device no longer supports the current increase and breaks down. Equivalently, since E and V are related by the distance between capacitor plates, it can also be referred to as a breakdown voltage (V_{BD}) measurement.
Ec+	value of electric field (E) in a polarization (P) versus E curve at crossing of the positive E-field axis
Ec–	value of electric field (E) in a polarization (P) versus E curve at crossing of the positive E-field axis
Fabry–Perot	of or related to a Fabry–Perot interferometry device or measurement.
Malvern	Panalytical X'pert3 CuKα X-ray diffractometer
MIM	metal-insulator-metal capacitor; in this study the piezoelectric properties of the PZT material are accessed for MEMS functionality
P_{Ar}	argon (partial) pressure
PCM	process control monitor, for monitoring the health of (one of the aspects of) the fabrication process

piezoMEMS	piezoelectric MEMS, system that uses a piezoelectric element to access the piezoelectric property to create the mechanical motion in response to the applied electrical signal
P_{DC}	DC power
P_{MAX}	maximum polarization
P_{MAX}	the maximum polarization (P) in a P versus E (electric field) or P versus V (voltage) plot
Pr	remnant polarization
Pr+	value of polarization (P) at crossing of the positive polarization axis
Pr-	value of polarization (P) at crossing of the negative polarization axis
PZT	lead zirconate titanate; $PbZr_xTi_{1-x}O_3$; in this study $x \approx 0.52$, near the PZT morphotropic phase boundary, where rhombohedral and tetragonal crystal symmetry overlap
R_a	average surface roughness, standard statistical definition relevant in this report to the AFM measurements
rotation speed	in this report, rotation speed is the rotation of the wafer about its central axis of symmetry during the sputtering deposition process
R_s	sheet resistance
R_{max}	maximum surface roughness, standard statistical definition relevant in this report to the AFM measurements
s	platinum film thickness
spectroscopic ellipsometry	thin-film thickness measurements which in this report were performed using a J.A. Woollam Model M-2000 F Spectroscopic Ellipsometer
soak	duration remaining in a condition, in this case at the stated temperature

T, TDEP, TPt	substrate temperature during deposition of the relevant thin film
tan δ	(or tan delta): loss tangent in dielectric capacitor measurements
V_{BD}	breakdown voltage
XRD	X-ray diffraction process and in this report X-ray diffraction measurements performed using the Malvern Panalytical X'pert3 CuKα X-ray diffractometer
Z	target substrate distance

1 (PDF) DEFENSE TECHNICAL INFORMATION CTR
DTIC OCA

1 (PDF) DEVCOM ARL
FCDD RLD DCI
TECH LIB

1 (PDF) FOX MATERIALS CONSULTING, LLC
GR FOX

28 (PDF) DEVCOM ARL
FCDD RLD
PJ BAKER
FCDD RLS
KA KAPPRA
AR SCHOFIELD
FCDD RLS E
RD DEL ROSARIO
FCDD RLS EM
CL MORRIS
FCDD RLS F
JA KROPP
JR MULCAHY
FCDD RLS G
RA BURKE
FCDD RLS S
WL BENARD
FCDD RLS SA
WC (KIRK) ALBERTS
RR BENOIT
SK ISAACSON
RR KNIGHT
JL MARTIN
RG POLCAWICH
DM POTREPKA
BK POWER
JM PUDER
JS PULSKAMP
RQ RUDY
NA STRNAD
FCDD RLS SE
ML CHIN
M DUBEY
S NAJMAEI
JS PEARSON
ML REED
WL SARNEY
FCDD RLS SQ
JF CHAN